TRIBHUVAN UNIVERSITY
INSTITUTE OF ENGINEERING
PULCHOWK CAMPUS

THESIS NO.: M-88-MSMDE-2020-2025

DYNAMIC MODELLING AND RESPONSE OF A CROSSFLOW TURBINE RUNNER

BY

LAL BABU PRASAD

A THESIS SUBMITTED TO THE DEPARTMENT OF MECHANICAL AND AEROSPACE ENGINEERING IN PARTIAL FULFILLMENT OF THE REQUIREMENTS FOR THE DEGREE OF MASTER OF SCIENCE IN MECHANICAL SYSTEM DESIGN AND ENGINEERING

DEPARTMENT OF MECHANICAL AND AEROSPACE ENGINEERING
LALITPUR, NEPAL

APRIL, 2025

TRIBHUVAN UNIVERSITY

INSTITUTE OF ENGINEERING

PULCHOWK CAMPUS

THESIS NO.: M-88-MSMDE-2020-2025

DYNAMIC MODELLING AND RESPONSE OF A CROSSFLOW TURBINE RUNNER

BY

LAL BABU PRASAD

A THESIS SUBMITTED TO THE DEPARTMENT OF MECHANICAL AND AEROSPACE ENGINEERING IN PARTIAL FULFILLMENT OF THE REQUIREMENTS FOR THE DEGREE OF MASTER OF SCIENCE IN MECHANICAL SYSTEM DESIGN AND ENGINEERING

DEPARTMENT OF MECHANICAL AND AEROSPACE ENGINEERING

LALITPUR, NEPAL

APRIL, 2025

COPYRIGHT

TRIBHUVAN UNIVERSITY
INSTITUTE OF ENGINEERING
PULCHOWK CAMPUS
DEPARTMENT OF MECHANICAL AND AEROSPACE ENGINEERING

The undersigned certify that they have read, and recommended to the Institute of Engineering for acceptance, a thesis entitled **"Dynamic Modeling and Response of a Crossflow Turbine Runner"** submitted by Lal Babu Prasad in partial fulfillment of the requirements for the degree of Master of Science in Mechanical System Design and Engineering.

Supervisor, Prof. Dr. Laxman Poudel
Department of Mechanical and Aerospace Engineering
IOE, Pulchowk Campus, TU

Supervisor, Asst.Prof. Laxman Motra
Department of Mechanical and Aerospace Engineering
IOE, Pulchowk Campus, TU

External Examiner, Asst.Prof. Manoj Adhikari
Department of Automobile and Mechanical Engineering
IOE, Thapathali Campus, TU

Committee Chairperson, Asst.Prof. Sudip Bhattrai, PhD
Head, Department of Mechanical and Aerospace Engineering
IOE, Pulchowk Campus, TU

Tribhuvan University
Institute of Engineering
Department of Mechanical and Aerospace Engineering
Pulchowk Campus

Date: April 07, 2025

ABSTRACT

The cross-flow turbine is a roto-dynamic hydraulic machine that share the common base with other machines or mounted close to each other which have also rotating shafts that share the some bearings. In this turbine hydraulic force is exerted two times in runner; once while the water enters the turbine and next when water leaves the turbine. The direction, amplitude and point of application of the forces in these two condition are very different, that is why it is obvious for vibrations. Due to external disturbance such as hydraulic force vector on the rotating runner and also some unbalanced potential, there is always possibility of vibration. In this work, the hydraulic force vectors that are applied on runner blades while water enters and exit have been determined by varying angle of attack and also by varying inlet blade angle. Governing equation of motion of the turbine runner has been developed assuming the runner shaft-disc attachment as flexible member. Modal analysis for low, medium and high spin speed range has been performed in ANSYS. Harmonic analysis has been done for various hydraulic force vectors that are caused by varying angle of attack and inlet blade angle. The maximum amplitude of the forced vibration verses attack angle and inlet blade angle has been determined and plotted. Finally, it is observed that the vibration amplitude increases with an increase in the inlet blade angle. Additionally, the amplitude initially rises with an increase in the angle of attack up to 20°, after which it begins to decrease with further increases in the angle of attack.. For the supplementary of the above work, the crossflow turbine runner has been designed, velocity triangles at inlet and exit of the turbine runner have been analyzed. For the analysis MATLAB program and ANSYS software have been used.

Keywords: *hydraulic force vectors, velocity triangles, maximum amplitude*

ACKNOWLEDGEMENT

At the very first, I express my sincerest gratefulness to my thesis supervisor, Prof. Dr. Laxman Poudel, for his supervision, guidance, encouragement and motivation throughout my research period and for providing me the chance to develop my research skills. I would offer my cordial gratitude to my thesis supervisor Asst. Prof. Laxman Motra who has supported me from the starting to the end of the project and guided me in each and every steps with his valuable knowledge and efforts. I express my deepest gratitude to my teacher Prof. Dr. Mahesh Chandra Luintel who provided me his valuable guidance and feedback, Without his proper guidance, this thesis might not have been completed.

I extend my special thank to Department of Mechanical and Aerospace Engineering, Pulchowk Campus for providing platform and facilities to conduct my research work. My special appreciation goes to all my teachers and colleagues whose discussions and suggestion enriched my understanding of the subject. finally I would acknowledge all those who contributed directly or indirectly to the completion of this thesis. your support and inspiration have made this work possible.

TABLE OF CONTENTS

LIST OF TABLES

LIST OF FIGURES

LIST OF SYMBOLS

D_o	Outer Diameter of Runner, m
D_i	Inner Diameter of Runner, m
H_g	Gross Head, m
α_1	Angle of attack at inlet of top blade
α_3	Angle of attack at second stage (bottom blade)
U_1	Circumferential velocity of runner at outer diameter, m/s
U_2	Circumferential velocity of runner at inner diameter, m/s
V_1	Absolute velocity at inlet of top blade, m/s
V_2	Absolute velocity at exit of top blade, m/s
V_3	Absolute velocity at inlet of bottom blade, m/s
V_4	Absolute velocity at exit of bottom blade, m/s
W_1	Relative velocity at inlet of top blade, m/s
W_2	Relative velocity at exit of top blade, m/s
W_3	Relative velocity at inlet of bottom blade, m/s
W_4	Relative velocity at exit of bottom blade, m/s
β_1	Angle between U_1 and V_1
β_2	Angle between U_2 and V_2
β_3	Angle between U_3 and V_3
β_4	Angle between U_4 and V_4
θ_1	Angle between relative velocity at inlet of top blade and x-direction
θ_2	Angle between relative velocity at exit of top blade and x-direction
θ_3	Angle between relative velocity at inlet of bottom blade and x-direction
θ_4	Angle between relative velocity at exit of bottom blade and x-direction
ρ_w	Density of water, kg/m^3
Ω	Spin speed of shaft, rad/s
ω_s	Angular velocity of the shaft, rad/s
ω_d	Angular velocity of the drum (Runner), rad/s
u	Displacement along x-axis
v	Displacement along y-axis

r_f	Position vector of any point of the flexible element
V_f	Velocity vector of any point of the flexible element
ω_f	Angular velocity vector of the flexible element
ρ_s	Density of shaft material, kg/m^3
ρ_d	Density of drum material, kg/m^3
A_s	Area of cross-section of shaft, m^2
A_d	Area of cross-section of drum, m^2
J_s	Polar second moment of area of shaft section, m^4
J_d	Polar second moment of area of drum section, m^4
I_s	Second moment of area of shaft section, m^4
I_d	Second moment of area of drum section, m^4
W_{hydf}	Work done due to hydraulic forces
$F_{xt}(t)$	Force exerted on top blade in x-direction
$F_{xb}(t)$	Force exerted on bottom blade in x-direction
$F_{yt}(t)$	Force exerted on top blade in y-direction
$F_{yb}(t)$	Force exerted on bottom blade in y-direction
$\mathcal{L}$	Lagrangian
KE_s	Kinetic energy of flexible shaft
KE_d	Kinetic energy of flexible drum
PE_s	Potential energy of flexible shaft
PE_d	Potential energy of flexible drum

CHAPTER ONE: INTRODUCTION

1.1. Background

In developing countries like Nepal, microhydropower schemes play a very important role in the development of the rural area through electrification energy programs. Micro-hydropower schemes can fulfill power requirement for small industries, agricultural and domestic uses through direct mechanical power or electrical power through coupling of turbine generator. Various types of hydraulic turbines, including Pelton, Crossflow, turgo and Kaplan turbines, are used in micro-hydropower plants. Among them, the Crossflow turbine is one of the most commonly used.

Most of the major micro hydro power plants in Nepal uses Crossflow turbine for power generation which are manufactured locally (1; 2) and suitability for low-head and medium-head water flows, which are common in the country. The mountainous terrain of Nepal and enough resources of water provide very good conditions for micro-hydropower and mini- hydropower, which makes crossflow turbines a critical technology for decentralized power generation and rural electrification.

Since the manufacturing cost of crossflow turbine is lower than that of pelton turbine, turgo turbine and kaplan turbine (2), it can be a practical and sustainable solution for micro-hydropower in Nepal. Combined support for community involvement, local manufacturing, skill development, and government policy will further enhance their contribution to the renewable energy resources of Nepal.

The cross-flow turbine is a rotodynamic hydraulic machine that may share the common base with generator, mounted close to each other, or in mechanical coupling systems that have rotating shafts sharing the same bearings, so it is obvious that vibrations suffer interference. Due to external disturbances as hydraulic force vectors on the rotating runner and also some unbalanced potential, there is always possibility of vibration. While vibration is a common issue also in crossflow tur-

bines, the study can be helpful in effective management through proper design, installation, and maintenance practices. Proactive monitoring and addressing the root causes of vibration not only improve turbine performance and operational lifespan but also ensure reliability and sustainability of power generation.

The dynamic behavior of the rotor, such as crossflow turbine runner can be studied and predicted to some extent by an appropriate analysis of their dynamic response through a proper mathematical modeling of the physical system (3), considering the interaction of hydraulic, mechanical, and structural dynamics. The dynamic response can also be determined by using simulation software like ANSYS. Such analysis can be helpful for predicting vibrations, optimizing design and ensuring stability during operation.

Many researchers have studied different aspects of these types of hydraulic power generation system to understand the dynamic behavior. They have performed such studies for Pelton turbines assuming its runner as rigid disc located at the center of simply supported flexible horizontal shaft, rigid disc at the end of horizontal overhanging shaft, and runner disc mounted in vertical shaft. Some studies have been also done for electrical generator assembly as flexible shaft and rigid disk. There are also some researches on dynamic response of gas and steam turbines. Similarly, some studies have been carried out for rigid bearings whereas some studies have also been carried out for flexible bearings. Similarly, flexible shafts have been modeled as either Euler-Bernoulli beams or as Timoshenko beams. Dynamic modeling of such shafts are usually performed for free as well as forced vibration for bending, torsional and longitudinal modes of vibration. For cross-flow turbine, many researchers have studied effect of on performance of the turbine at various operating condition and design parameters. These operation condition and design parameters includes speed of the turbine, angle of attack, inlet and exit blade angle, dimeters ratio, radius of curvature of blade.

Modal Analysis of a Crossflow Turbine runner focuses on determining its natural frequencies, mode shapes and critical speed to understand how the turbine structure can respond to dynamic forces. This is critical for avoiding resonance, min-

imizing vibrations. Harmonic analysis of a crossflow turbine runner investigates how it responds to periodic forces, especially those caused by hydraulic forcing vector at different circumferential of runner position. Further, the harmonic analysis of the turbine runner at different forcing vector for varying angles of attack and inlet blade angles may facilitate to choose appropriate value to reduce vibration.

1.2. Problem Statement

Most of the researches on the dynamic behavior of rotor dynamics has been carried out on modeling of systems such as flexible shaft, flexible disk, and shaft-disk assembly. There are also some similar researches on dynamic response of gas turbines, steam turbines and generator assembly. Although few researchers have worked on the dynamics response of water turbines and they have focused on modeling of Pelton turbine.

For cross-flow turbine, many researchers have studied effect on performance of the turbine at various operating conditions and design parameters includes speed of the turbine, angle of attack, inlet and exit blade angle, diameters ratio, radius of curvature of blade.

This research is focused on the dynamic modeling of the crossflow turbine runner, modal analysis of the turbine runner and harmonic analysis for different hydraulic forcing vector at various angle of attack and blade inlet angle by using simulation software. The modeling and analysis will cover the dynamic behavior of the shaft and the runner drum at different design parameters like angle of attack and blade inlet angle.

1.3. Research Objectives

1.3.1. Main Objective:

The main objective of this study is to develop a mathematical model of the cross-flow turbine runner assembly, conduct a modal analysis of the turbine runner, and perform harmonic analysis under varying hydraulic forcing vectors influenced by changes in the angle of attack and blade inlet angle.

1.3.2. Specific Objectives

- To design runner of crossflow turbine.
- To analyze the hydraulic force vectors using the velocity triangle.
- To develop governing equation of motion for the turbine runner-shaft assembly.
- To conduct modal analysis on ANSYS.
- To perform harmonic analysis at different hydraulic forcing vector due to varying angle of attack and blade inlet angle.

1.4. Scope of the Work and Assumptions

The scope of this study involves developing a comprehensive mathematical model of the crossflow turbine runner assembly, focusing on its structural and dynamic characteristics. The study aims to perform a modal analysis to identify the natural frequencies and mode shapes of the turbine runner, which is crucial for evaluating resonance risks during operation. Additionally, a harmonic analysis will be conducted to assess the turbine's response to hydraulic forcing vectors under varying angles of attack and blade inlet angles. This analysis will quantify dynamic stresses and displacements to ensure the structural integrity of the runner under variation in the design parameter and operating condition. By addressing these aspects, the study seeks to improve the understanding of the turbine's dynamic behavior and contribute to the optimization of its design for improved performance and durability. Ultimately, the findings could serve as a reference for advancing crossflow turbine technology and improving its application in renewable energy systems.
The following assumptions are taken for the development and analysis of the model:

- Water enters and exit at atmospheric pressure.

- Secondary forces, such as turbulence-induced forces and drag forces, are not included.
- Bearings are rigid.
- The turbine operates at its synchronous speed with the designed flow rate.
- There is no longitudinal displacement at any point on the shaft.

CHAPTER TWO: LITERATURE REVIEW

2.1. Construction and Working principle of Crossflow Turbine

Cross-flow turbines are classified into a set of impulse turbines. The most important reason for such a classification is that these turbines operate in the air and do not submerge like reaction turbines. The set operates at atmospheric pressure. The Crossflow turbine has a drum-shaped rotor with fixed disks at both ends, and trough-designed buckets connect the two disks. The water is drawn from the inlet guide to the rotor. The inlet guide guides the water under pressure to the rotor for the first time and transfers the impulse force inside the drum. After this process, the water passes through the rotor and leaves the turbine at ambient pressure. The cross-flow turbine then changes the water pressure and converts it into mechanical energy. This effect reduces the pressure drop in a very small amount across the buckets of the turbine and improves efficiency. Most of the energy extracted from the top buckets (around 72%) and the remaining 28% from the bottom buckets.(4)

The angular momentum of the water flowing through the turbine rotor buckets converts the kinetic energy of the water into torque on the output shaft, with which the generator can be driven in a small hydroelectric system.

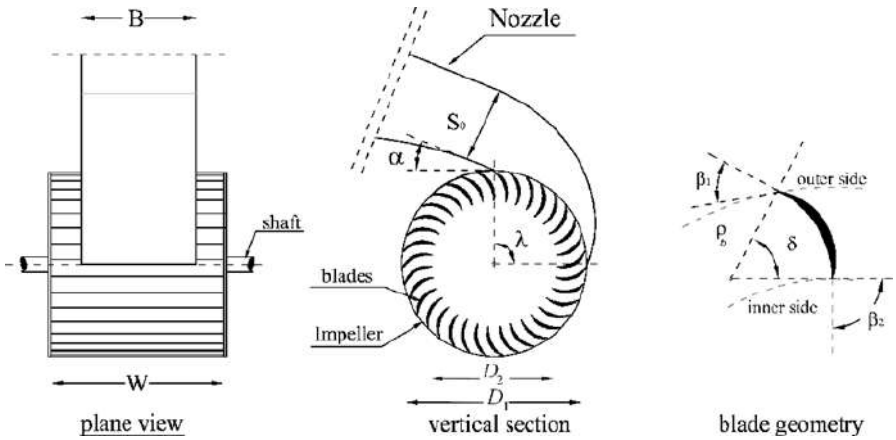

Figure 2.1 A typical Cross flow Turbine layout

2.2. Velocity Triangle of Crossflow Turbine Runner

The velocity triangle in a crossflow turbine describes the interaction between water flow and the rotating runner blades, providing information on the energy transfer mechanism. A crossflow turbine operates by directing water through a nozzle to strike the turbine blades at an angle, where energy conversion takes place. The velocity triangle is used to analyze the relative motion of the water and turbine blades at both the inlet and outlet of the runner.

At the inlet, water enters the runner with an absolute velocity V_1 at an angle α_1 to the tangential direction of the blade. The tangential velocity of the runner blade U_1 depends on the rotational speed and radius of the turbine. The relative velocity W_1 represents the velocity of the water relative to the blade, and forms the inlet velocity triangle. Inlet angles and velocities are critical for ensuring efficient energy transfer during the initial interaction.

At the outlet, after the first stage of interaction with the runner blades, the water exits with a reduced absolute velocity V_2 and a different angle α_2. The relative velocity at the outlet W_2 is determined by the blade geometry and the flow conditions. The outlet velocity triangle helps to understand the remaining energy in the water and optimize the turbine design for maximum efficiency.

Similarly in the second stage, the velocity triangles are formed at entry by absolute velocity V_3, tangential velocity of the runner blade U_3, relative velocity W_3, and at the exit by absolute velocity V_4, tangential velocity of the runner blade U_4, relative velocity W_4.

A distinctive feature of the crossflow turbine is its two-stage energy transfer process. After exiting the first stage, water reenters the runner at a different angle and strikes the blades again for additional energy extraction. This secondary interaction results in separate velocity triangles for the first and second stages, reflecting the complex flow dynamics. These velocity triangles are fundamental for analyzing the forces on the blades, optimizing the angle of attack, and determining the efficiency of energy conversion in a crossflow turbine.

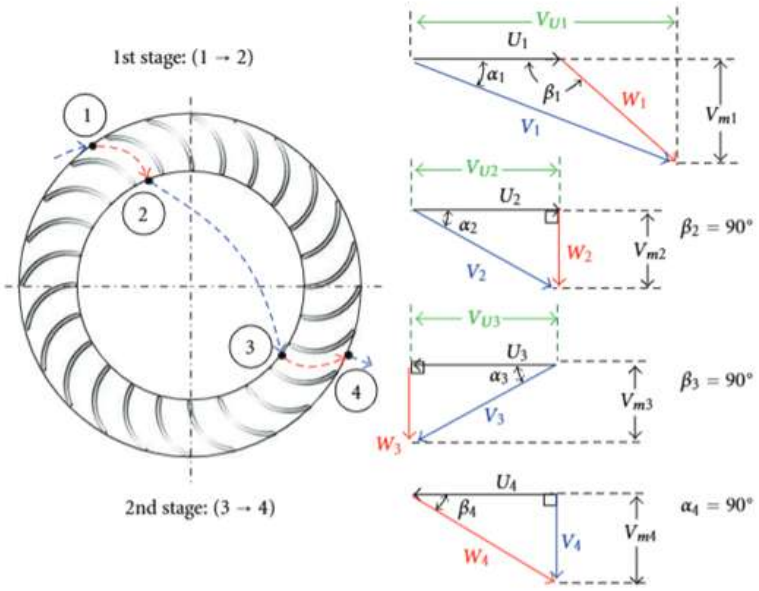

Figure 2.2 Theoretical Velocity Triangle of Cross-flow Turbine Runner

2.3. Crossflow Turbine Runner Model

A crossflow turbine rotor consists of a drum-shaped runner with a nos. of semi-circular blades fixed circumferentially on two circular plates on both sides. The runner is attached at the mid shaft supported by bearings at the ends.

A rotodynamic system can be modeled using two main approaches: the discrete parameter model and the distributed parameter (or continuous) model. The discrete parameter method uses lumped or consistent mass representations, often considering the shaft as massless. On the other hand, the distributed parameter approach models the shaft as a rotating beam, applying either Euler-Bernoulli or Timoshenko beam theories. In Euler – Bernoulli beam theory, shear deformations are not taken, the deformed beam angles are very small, and the plane sections remain plane and parallel to the transverse axis. In the Timoshenko beam theory, plane sections still remain plane but are no longer parallel to the transverse axis. The selection of a suitable modeling approach depends on how complex the system is. For relatively simple systems, a continuous model may be used directly. However, when dealing with more complex systems, it is generally more practical to adopt a discrete parameter model. The equations of motion for such systems

can be formulated using Newton's second law, the method of equivalent system parameters, or the principle of energy conservation. These techniques are particularly effective for discrete systems with a limited number of degrees of freedom. For systems with a higher number of degrees of freedom, whether discrete or continuous, equations of motion can also be developed using energy-based approaches or variational principles. Among the most widely used variational methods are the Hamilton principle and the Lagrange equations, both of which are advanced formulations derived from Newton's second law.

2.4. Some Terminologies in Rotodynamics

2.4.1. Whirling

Due to centrifugal or centripetal forces, a rotating rotor tends to bend and move in an orbital or elliptical path, a phenomenon known as whirling. The whirling frequency is influenced by the rotor's stiffness and damping, similarly to the free vibration behavior of any dynamic system. Whirling can occur in two forms: forward or backward, as illustrated in figure 2.3. Forward whirling occurs when the rotor's deformation moves in the same direction as its rotation, while backward whirling occurs when the deformation opposes the rotational direction.

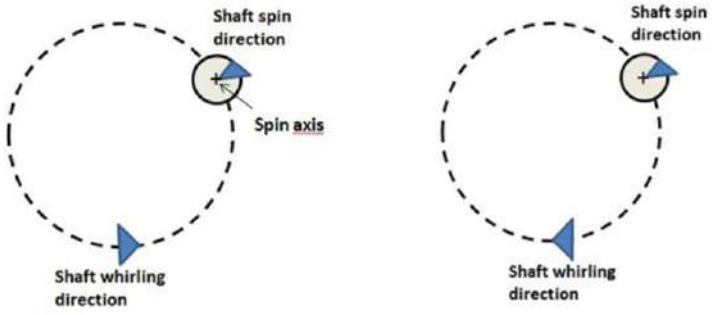

Figure 2.3 Types of Whirling

2.4.2. Damping

Damping refers to a system's capacity to dissipate energy, thereby limiting dynamic response and preventing excessive vibration amplitudes caused by forced

resonance or self-excited oscillations. In rotor systems, the damping can be classified as internal or external.

• Internal damping arises from rotating components, primarily due to material hysteresis.

• External damping is introduced by stationary elements, such as bearings and support structures.

The stability of a rotor system is heavily dependent on its damping characteristics: higher damping generally enhances stability by suppressing vibrational growth. Internal damping is undesirable because it decreases the stability of the system, but external damping limits the amplitude, stabilizes the system, and also increases somewhat critical speed.

2.4.3. Mode Shapes

Mode shapes represent the characteristic patterns of deformation or vibration that a structure or system exhibits when vibrating at its natural frequencies. Each mode shape corresponds to a specific natural frequency and illustrates the relative displacement of the structure components during vibration. These shapes depend on the geometry, material properties, and the boundary conditions of the system, providing information on how it responds to dynamic forces. Mode shapes are independent of vibration amplitude, showing only the relative movement of points, and are typically orthogonal to one another in mathematical terms. They play a crucial role in engineering applications, such as predicting how buildings, bridges, or machinery respond to dynamic loads, and are essential to avoid resonant frequencies that could lead to structural failure. By analyzing mode shapes, engineers can optimize designs, ensure structural safety, and refine models through experimental validation techniques such as modal testing.

2.4.4. Critical Speed

The operating speed at which the excitation frequency of a rotating system becomes equal to any one of the natural frequencies is called the critical speed. At

critical speeds, the vibration amplitude of the system can increase drastically and become excessive, potentially causing damage or failure.

When a rotating system operates at or near its critical speed, the centrifugal forces amplify deflections, leading to increased vibrations. This occurs because the natural frequency of the system matches the excitation frequency caused by its rotation. Factors such as mass distribution, stiffness, damping, and boundary conditions influence the critical speed. The critical speed is obtained by creating a Campbell diagram.

2.4.5. Campbell Diagram

The Campbell diagram visually depicts the relationship between the natural frequencies of a system and the excitation frequencies, which vary with rotational speed. A typical Campbell diagram is illustrated in figure 2.4. The x-axis represents the rotor's rotational speed, and the y-axis shows the system's natural frequencies, calculated across different operational speed ranges. A key feature of the diagram is the excitation line, which corresponds to the rotor's rotational frequency. The critical speed is identified at the intersection point where the excitation line crosses a modal frequency line, indicating a potential resonance condition.

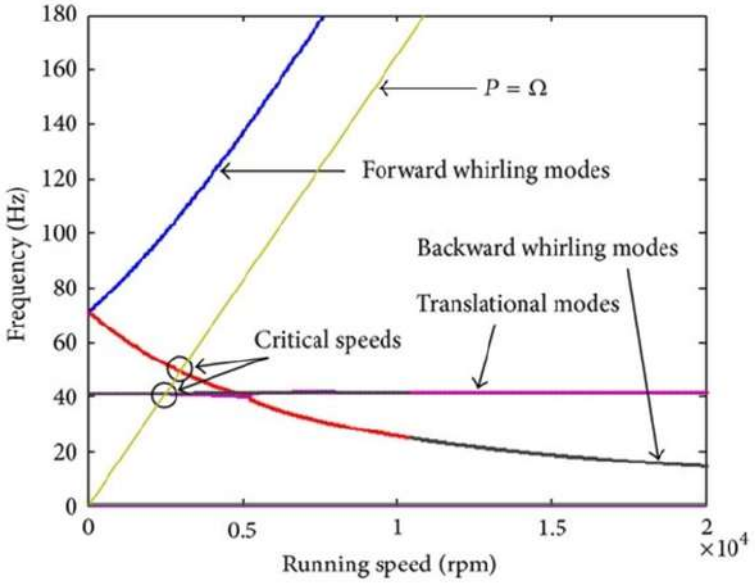

Figure 2.4 Typical Campbell diagram

2.4.6. Coriolis Effect

The Coriolis force is an apparent inertial force that acts on objects moving within a rotating reference frame, deflecting their path perpendicular to both the rotation axis and the velocity of the object. In clockwise rotating systems, this deflection occurs to the left of the motion, while in counterclockwise rotating systems, it deflects to the right, the phenomenon is known as the Coriolis effect. The magnitude of this force depends on the object's speed relative to the rotating frame, specifically its velocity component orthogonal to the axis of rotation. In rotor systems, the Coriolis effect causes natural frequency splitting, leading to additional resonance conditions that influence vibrational behavior and stability.

In the context of vibrations, the Coriolis effect refers to the additional forces and effects experienced in a rotating reference frame, such as in rotating machinery or gyroscopic systems. When a vibrating object or particle moves within a rotating system, the Coriolis effect introduces a force that is perpendicular to both the direction of the vibration and the axis of rotation. This phenomenon arises due to the rotation of the reference frame and has significant implications for the dynamics and stability of rotating systems.

2.5. Literature Survey

The dynamic behavior of this crossflow turbine runner depends on many factors such as the arrangement of the impeller blades, the water flow pattern, and the operating conditions. Many researchers have studied dynamic modeling of similar systems in the equivalence of the shaft-disc or shaft-drum arrangement also with interaction with bearing. Some researchers have also considered different types of motion in addition to spin and also forcing vectors. Some researchers also studied the dynamic behavior of different types of turbine such as Pelton turbine, Francis turbine, propeller turbine, Kaplan turbine, gas turbine, and steam turbine. Many researchers have modeled such types of system by simulation, and some have also done mathematical modeling.

For cross-flow turbine, researchers have also studied effect on performance of the turbine at various operating conditions and design parameters that includes speed of the turbine, angle of attack, inlet and exit blade angle, diameters ratio, radius of curvature of blade.

Some relevant researches related to this proposed research are given here.

J. ˇSaˇsek et al. have employed a one-dimensional continuum representation of the shaft based on the Bernoulli-Euler beam theory. This approach relies on the key kinematic assumption that cross sections remain planar and normal to the shaft's neutral axis throughout vibrational deformation. Disks are modelled as a three dimensional continuum by means of the finite element method. (5)

Naim Khader et al. experimentally investigated the vibrational characteristics of a flexible shaft system incorporating multiple compliant disks, determining its natural frequencies through systematic testing. The experimental results are compared with the corresponding results, obtained from a theoretical study, based on the assumed mode method, with the free vibration mode shapes of the system's individual components, i.e., flexible shaft and flexible disks, considered as the assumed functions. (6)

Yong do chui et al. have studied the effect of blade angle on the performance of a cross-flow turbine. The analysis of turbine performance for power generation

and efficiency have been done for various inlet and outlet blade angle by using commercial CFD code. (7)

Srikrishnanivas developed an ANSYS-based model of an RM12 jet engine rotor and analyzed its rotordynamic performance using Dyrobes, a specialized rotordynamics analysis software. He has done modal analysis for mode shapes and respective natural frequencies using ANSYS software. He has also performed post-processing of the simulation work by using ANSYS. (8)

(Shi et al. have performed dynamic modeling and analysis of wind turbine using torsional dynamic model. The researchers formulated a mathematical representation of a horizontal-axis wind turbine drivetrain system utilizing a multi-body torsional dynamics modeling approach. They derived the governing equation by using the Lagrange's equation, which takes into account the kinetic and potential energies and the work from the input torque, and solved the governing equation numerically by direct numerical integration. (9)

Huang et al., in their research work on dynamic behavior of pump-turbine runner, have carried out numerical simulation and experimental measurement to determine dynamic behavior of circular disc-blade structure and have compared the simulation result and experimental result. (10)

Khan & Badshah have done model analysis of crossflow turbine to determine mode shape and respective natural frequencies by using ANSYS 13 in his study of Design and Analysis of Cross Flow Turbine for Micro Hydro Power Application using Sewerage Water. (11)

Mirtalaie & Hajabasi have performed the linear lateral free vibration analysis of the rotor is performed based on the Timoshenko beam theory including the effects of rotary inertia, gyroscopic effects, and shear deformations. They have investigated the free vibration behavior of parametrically excited system by perturbation method and compared with the common Rayleigh, Timoshenko, and higher-order shear deformable spinning beam models in the rotor dynamics. (12)

Manchan Tiwari & Rajendra Shrestha investigated how design parameter variations influence the efficiency of cross-flow turbines through ANSYS-based sim-

ulations under steady-state conditions. Their numerical results were validated against operational data from field installations where the turbine designs were implemented. Different Cross flow turbine models were prepared by varying the curvature radius of the blade and the ratio of inner to outer radius of the runner(1). Warjito et al. conducted a comparative CFD analysis of blade design performance in cross-flow turbines, examining NACA-6712 airfoil profiled blades against conventional blade designs. Their numerical study implemented the SST turbulence model in ANSYS Fluent 17 to systematically evaluate the aerodynamic differences between these blade configurations. From the results, it has been obtained that the ordinary turbine is better than NACA-6712 turbine. (13)

Motra & Luintel developed a computational model of a Pelton turbine featuring a rigid, centrally mounted runner supported by simple rigid bearings. The researchers derived the system's governing equations through Lagrange's formulation and employed analytical solution techniques using the Rayleigh-Ritz method to determine natural frequencies. Their study presents a comparative analysis between the critical frequencies identified for discrete systems with equivalent mass representations and those predicted by a continuous modeling approach. (3)

Luintel investigated Pelton turbine runner dynamics through free and forced vibration analyses, modeling the system as a rigid disk on a flexible shaft. Using rotating Euler-Bernoulli and Timoshenko beam theories, he derived equations of motion, computed critical speeds, and evaluated water jet-induced transverse vibrations. The study compared both models' predictions of natural frequencies and forced responses, with the forced vibration results further validated against experimental data. (14)

Mohammed Khair et al. analyzed the vibration transmission and frequency response of a flexible shaft-disk rotor supported by nonlinear bearings. The researchers modeled the system's elastic deformations using the Assumed Modes Method and derived the equations of motion through Lagrange's energy-based approach. Their study focused on characterizing both the force transmissibility through the nonlinear suspension and the system's dynamic response under

operational conditions. The Harmonic Balance (HB) method combined with a continuation scheme is used to determine the nonlinear frequency response and force transmissibility curves due to disk unbalance force. (15)

Koirala & Luitel have studied the dynamic response of the vertical shaft of a Pelton turbine. They have modeled the equation of motion by using Hamilton's Principle and and have solved the equation by Galerkin method for angular velocity. They have compared the analytically calculated frequency with the ANSYS simulated result. (16)

Zhang & Chen have done experimental and numerical investigations of the modal and dynamic behavior of a prototype Kaplan turbine runner. They have performed modal analysis and harmonic analysis by using ANSYS 16.2 software and have compared the result with experimental model analysis. (17)

Pandey analyzed transient vibrations in a cantilever shaft-disk system under water jet impact, resembling Pelton turbine conditions. The study developed a mathematical model, solved the governing equations for the first three modes using MATLAB, and validated the results with ANSYS simulations. This work provides key insights into transient responses during turbine startup and shutdown. (18)

Madhav Baral et al.investigated the modal characteristics of a hydro generator rotor system supported on elastic bearings, employing the transfer matrix method for natural frequency analysis of transverse vibrations. Their analytical approach incorporated both Euler-Bernoulli and Timoshenko beam theories to formulate the shaft's transfer matrix, enabling comparative evaluation of these theoretical frameworks for rotating system dynamics. The solutions obtained with these considerations have been compared with the results obtained from the Finite Element method (FEM) to evaluate the reliability of the mathematical approach. (19)

2.6. Research Gap

The existing studies on dynamic behavior of hydraulic turbines are mainly focused on pelton turbine. Previous studies on crossflow turbines have focused on design

and performance analysis, and there is limited research on modal analysis. Furthermore, no studies have developed a mathematical model of a crossflow turbine runner that can be helpful to predict the dynamic behavior. This research aims to bridge these gaps by developing a mathematical model for the governing equation of motion of a crossflow turbine runner. It also conducts modal analysis to determine natural frequencies, mode shapes, and critical speeds, which are crucial for avoiding resonance. Furthermore, harmonic analysis of the crossflow turbine runner investigates how it responds to periodic forces, especially those caused by hydraulic force vector for varying angles of attack and inlet blade angles that may facilitate to choose appropriate value of these angle to reduce vibration.

CHAPTER THREE: RESEARCH METHODOLOGY

3.1. Thesis Framework

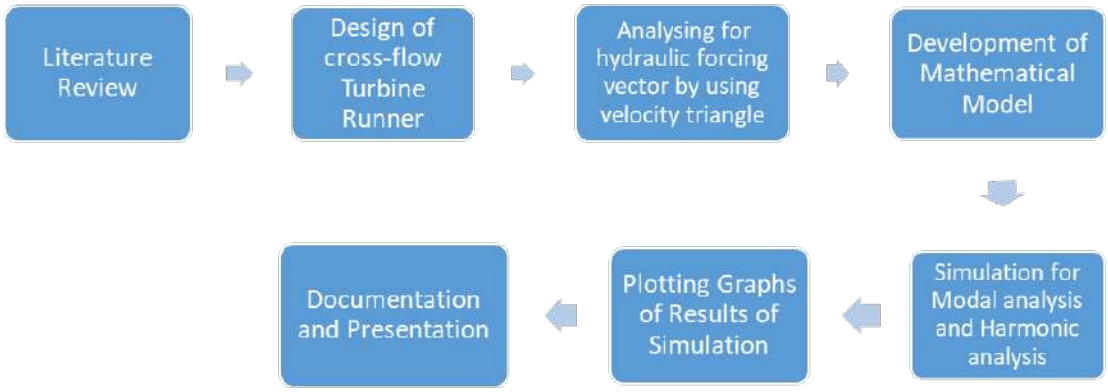

Figure 3.1 Flowchart of research methodology

3.2. Literature Review

The past research works and other literature related to this research work are collected from the library and the Internet. The past thesis of the Institute of Engineering and their access to many international journals are studied. The related earlier literature is also studied, categorized according to the nature of problem they focused on, the methodology they adopted, and their major findings are extensively reviewed.

3.3. Design of Cross Flow Turbine Runner

The schematic diagram of the turbine used in the study is mentioned in figure 3.2. The outer diameter, inner diameter, jet dimension, blade thickness, blade spacing, and nos. blades are determined. The runner width is assumed according to the manufacturer's recommendation (Lumbini Engineering & Hydropower) as listed in table 3.1. Similarly, the design flow rate, RPM and head are adopted as

specified by the manufacturer, as in the table 3.1.

Table 3.1 Design Parameters of the Crossflow Turbine

S.N.	Given Parameter	Value
1	Gross Head (H_g)	47 m
2	Design Flow Rate (Q_{design})	0.116 m^3/s
3	RPM (N)	850
4	Runner Width (B)	83 mm

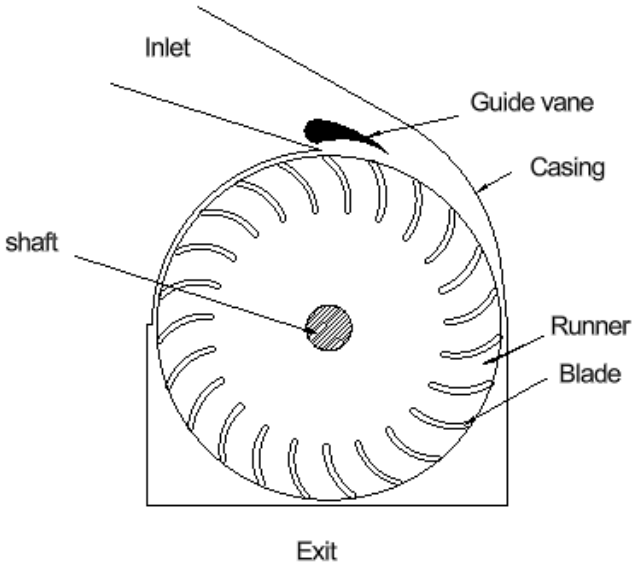

Figure 3.2 Schematic diagram of crowwflow turbine

3.4. Analysis of Hydraulic Force vector

The crossflow turbine works at atmospheric pressure; hence the hydraulic force exerted on the runner is only an impulse force. At constant mass flow rate, the impulse force exerted by the water depends on the change in the velocity vector of the water while passing through the runner. The velocity vectors at entrance and exit at the first stage attack and at the second stage attack are analyzed using the velocity triangles of the crossflow runner, and are used to determine hydraulic force vector. Here after the first stage is represented by the top blade, and the

second stage is represented by the bottom blade. The x and y components of the hydraulic force acting on the top and bottom blades are determined using MATLAB for various angles of attack and inlet blade angles while keeping other design parameters constant.

3.5. Mathematical Model Development

Mathematical model of the crossflow turbine is developed assuming a flexible shaft and drum where the drum has equivalent mass of the runner. The drum-shaft assembly is assumed to be simply supported with bearings at both ends with the drum in the middle. The kinetic energy and potential energy of both the shaft and the drum are derived. The problem is formulated using the Euler-Bernoulli beam model. The equation of motion is derived using the Hamilton's principle as follows: (20)

$$\int_{t_1}^{t_2} (\delta\mathcal{L} + \delta W_{\text{hydf}})\, dt = 0$$

Where $\mathcal{L}$ is known as a Lagrangian functional and W_{hydf} is the virtual work due to all the non-conservative forces.

And, $\mathcal{L}$ =KE - PE

The kinetic energy (KE) of a rotating flexible shaft-drum system is given by (14):

$$KE = \frac{1}{2}\rho A \int_0^L \left[(\dot{u} - \Omega v)^2 + (\dot{v} + \Omega u)^2\right] dz + \frac{1}{2}\rho J \int_0^L \left[(\Omega + u'\dot{v}')^2\right] dz + \frac{1}{2}\rho I \int_0^L \left[(-\Omega u' - \dot{v}')^2 + (-\Omega v' + \dot{u}')^2\right] dz$$

The potential energy (PE) due to bending deformation is expressed as (14):

$$PE = \frac{1}{2} EI \int_0^L \left[(u'')^2 + (v'')^2\right] dz$$

where ρ is the material density, E is the elastic modulus, A is the cross-sectional area, u, v, w are displacement components, I is the area moment of inertia, ω is the angular velocity, and L is the shaft length.

3.6. Simulation Work

The geometry of the crossflow runner turbine is modeled in AutoCAD with the dimension achieved by the design. The simulation work for the modal analysis and the harmonic analysis of the runner is done in ANSYS Workbench by applying engineering data for the chosen material stainless steel. Harmonic analysis of the runner is done for various force vector.

3.6.1. Modal Analysis

The numerical analysis utilizes ANSYS's built-in engineering material library, with stainless steel selected for its mechanical properties. The geometric model, imported in IGES format from AutoCAD, features a shaft assembly with rigid bearing supports modeled by applying extremely high stiffness values at both ends. A refined mesh was generated with controlled element quality to ensure solution accuracy. Boundary conditions were implemented using remote displacement constraints, allowing rotational freedom about the longitudinal axis while preventing axial displacement. Three spin speed; 0 rad/s, 44.5 rad/s, and 100 rad/s, is given where 44.5 rad /s is its steady condition operational velocity. The model is solved for maximum 12 modes and 3 nos. of point in rotodynamic control. The solution developed 36 nos. of total deformation and also the Campbell Diagram. Since single and very low critical speed is achieved in low spin speed range, again the model analysis done for high range of spin speed, from 100 rad/s to 1000 rad/s and from 1000 rad/s to 5000 rad/s with all the parameters constant.

3.6.2. Harmonic Analysis

Harmonic analysis is conducted for the same analyzed modal of low speed range. Analysis setting is done for linear frequency spacing ranging from 0 Hz to 100 Hz with 10 nos. of solution interval. force vector is defined as x-component and y-component at mid-point of the top blade for and separately at mid-point of the bottom blade. There are nine sets of force vectors obtained by varying the angle

of attack, and another nine sets obtained by varying the inlet blade angle. The solution provided frequency response graphs with amplitude vs. frequency up to 10 points for both x-direction and y-direction and also phase angle vs. frequency. From frequency response of harmonic analysis the maximum amplitude at various force vectors is tabulated, and graphs of maximum amplitude vs. its respective causal angles are plotted by programming in MATLAB.

3.7. Result

The mathematical governing equation of motion of the turbine runner is obtained as coupled linear differential equation with is boundary condition. The modal analysis determined natural frequencies for different vibration modes at low and high rotational velocities. A single low critical speed was observed at low velocities, while multiple critical speeds appeared at higher velocities. Harmonic analysis provided frequency response data, identifying maximum amplitudes for various force vectors. MATLAB plots of the maximum amplitude vs. causal angles revealed the influence of force vector variations on the system response.

3.8. Documentation

This comprehensive study is documented in a six-chapter format, systematically organized from foundational concepts to final outcomes. Chapter 1 introduces the research context, presenting the background, problem statement, objectives, scope, and key assumptions. Chapter 2 critically examines existing literature while identifying gaps in current knowledge. The methodology is thoroughly detailed in Chapter 3, followed by Chapter 4's presentation of the design process, mathematical modeling, and simulation analysis. Chapter 5 analyzes and interprets the results obtained from both analytical and computational approaches. The final chapter (Chapter 6) synthesizes the study's conclusions, summarizing key findings and their implications.

CHAPTER FOUR: DESIGN, MATHEMATICAL MODEL

DEVELOPMENT AND ANALYSIS

4.1. Design of Crossflow Turbine Runner

4.1.1. Runner Diameter and Jet Thickness

For the given gross head (H_g) and the required RPM, the outer diameter of the runner is determined as:

$Do = \frac{30\sqrt{2gH_g}}{\pi N} \cos\alpha_1$ (21)

Taking $\alpha_1 = 22°$, suggested by (22; 23) for maximum efficiency,

$$Do = 0.31 \approx 0.3\ m$$

The runner has two diameters, outer and inner. The inner diameter,

D_i =0.68 D_o (22; 21) = 0. 204 m.

Taking the runner width of 83 mm, the thickness of the jet t_j is given by

$t_j = \frac{Q_{design}}{B\times\sqrt{(2gH_g)}}$ (22; 21) = 47.77 ≈ 48 mm

4.1.2. Runner Blade

For blade inlet angle at first stage,

$\tan\beta_1 = 2tan\alpha_1$ $\beta_1 = 39°$

Taking the blade inlet angle, β_1=39^0, the blade spacing, t_s is given by:

$t_s = \frac{K\ \times D_o}{sin\beta 1}$ (23).

The nos. of blades is given by $n_{b=}$ $\frac{\pi\times D_o}{t_b}$ =22.72 ≈ 23 (23)

The radius of curvature of blade, r_c is given by:

$r_c = \frac{D_o}{4}[1 - (\frac{D_i}{D_o})^2]/\cos^{-1}\ \beta_1$ (23) = 51.89 ≈ 52 mm

Blade thickness, $t_b = 0.0017 \times D_o$ (11) $= 5.1 \approx 5$ mm

4.2. Analysis of Velocity Triangle

U, V and W are the circumferential velocity of the runner, the absolute velocity of water, and the relative velocity of water along the blade, respectively. α is angle of attack and β is the angle between U and W. The suffix 1 & 2 are for inlet and exit at the top blade, i.e. at first stage, and that 3 & 4 are for inlet and exit at the bottom blade, i.e., at second stage. The following relations between these velocities are used in MATLAB programming to calculate the force vector.

$U_1 = \frac{N \times \pi \times D_o}{60} = 13.35$ m/s

$V_1 = \sqrt{2gH_g} = 29.25$ m/s

For maximum efficiency, $\alpha_1 = 22°$ (23)

$\tan \beta_1 = 2tan\alpha_1 \ \beta_1 = 39°$

$V_1 \cos \alpha_1 = U_1 + W_1 \cos \beta_1$

$W_1 = \frac{V_1 \cos \alpha_1 - U_1}{\cos \beta_1}$

$U_2 = \frac{N \times \pi \times D_i}{60}$

$W_2 = \sqrt{(W_1^2 - U_1^2 + U_2^2)}$

$\tan \alpha_2 = \frac{W_2}{U_2}$

$\alpha_2 = \tan^{-1} \frac{W_2}{U_2}$

$V_2 = \sqrt{(W_2^2 + U_2^2)}$

The angular displacement (γ_r) of the runner when water travels from the outer radius of runner to the inner radius along the blade,

$\gamma_r = \frac{(1 - \frac{D_i}{D_o}) U_1 \times 360°}{V_2 \times 2\pi}$ (24)

The angular position of exit of water from the top blade.

$\psi = \gamma_r + \phi$

Where ϕ is angle subtended by ends of the runner blades at center of the runner

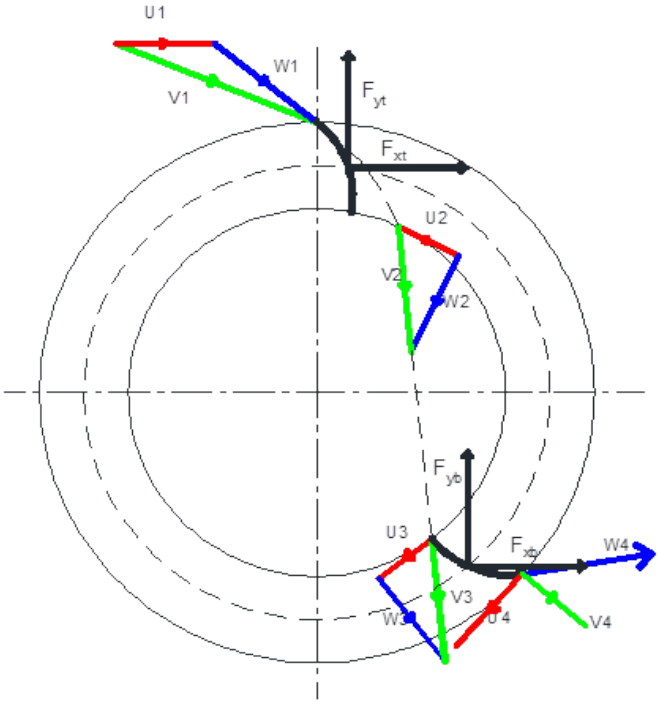

Figure 4.1 Diagram of velocity triangle in actual magnitude and direction line scale

that has been graphically determined to be 11° which is also angular position of lower tip of blade at initial state.

$U_3 = U_2$

$V_3 = V_2$

$\alpha_3 = \alpha_2$

$W_3 = \sqrt{(V_3^2 - U_3^2)}$

$\beta_4 = 180° - \beta_1$

$U_4 = U_1$

$W_4 = W_1$

$V_4 = \sqrt{(W_4^2 + U_4^2 + 2\, W_4\, U_4 \cos \beta_4)}$

$V_4 \cos \alpha_4 = U_1 - W_1 \cos \beta_1$

$\alpha_4 = \cos^{-1}\left(\frac{U_1 - W_1 \cos \beta_1}{V_4}\right)$

4.3. Hydraulic Force Vector

Since the turbine operates at atmospheric pressure, the hydraulic force exerted on the runner blades only depend on change in momentum of water flowing along the blades. The water exerts force on the runner blades two times, once while entering in runner which is called first stage and next while leaving the runner which is called second stage.

From the figure 4.1 of velocity diagram assuming direction of x-coordinate positive towards right direction and y-coordinate positive in upward direction. The angle made by relative velocities W_1, W_2, W_3 and W_4 with positive x direction are:

$\theta_1 = \beta_1$

$\theta_2 = \psi + 90°$

$\theta_3 = 2\alpha_2 + \psi - 90°$

$\theta_4 = 2\alpha_2 + \psi - \phi - \beta_4$

Hence the x and y components of hydraulic force exerted on the top blade and bottom blade are calculated as:

On top blade,

x- Component of the force, $F_{xt} = \rho_w Q_{design} (W_1 \cos\ \theta_1 - W_2 \cos\ \theta_2)$

y- Component of the force, $F_{yt} = -\rho_w Q_{design} (W_1 \sin\ \theta_1 - W_2 \sin\ \theta_2)$

Resultant force on the top blade, $F_t = \sqrt{{F_{xt}}^2 + {F_{yt}}^2}$

On the bottom blade,

x- Component of the force, $F_{xb} = \rho_w Q_{design} (W_3 \cos\ \theta_3 - W_4 \cos\theta_4\ )$

y- Component of the force, $F_{yb} = -\rho_w Q_{design} (W_3 \sin\theta_3\ \ - W_4 \sin\ \theta_4)$

Resultant force on the bottom blade, $F_b = \sqrt{{F_{xb}}^2 + {F_{yb}}^2}$

4.4. Hydraulic Force Vector at Various Angle of attack and Blade Inlet Angle

The x-component and y-component of the hydraulic force exerted by water on the top blade i.e. at first stage and that at bottom i.e. at second stage with varying angle of attack from 0° to 80° at interval of 10° keeping value of other parameter same as designed, was determined by using MATLAB program. Similarly, these component of forces were also determined for various blade inlet angle from 0° to 80° at interval of 10° keeping value of other parameter same as designed.

The table 4.1 below shows x and y components of hydraulic forces on top blade i.e. at first stage and that on bottom blade i.e. at second stage, at different angle of attack keeping the other parameter same as designed.

Table 4.1 X and Y components of hydraulic forces at varying attack angle

S.N.	Attack angle(α_1)	Angular speed rad/s	$F_{xt}(N)$	$F_{yt}(N)$	$F_{xb}(N)$	$F_{yb}(N)$	Remark
1	0 °	48.76	2274.9	998.58	444.32	-2181.8	
2	10 °	48.02	2289.6	531.31	-194.43	-2018.8	
3	20 °	45.81	2295.8	264.43	-810.36	-1761.5	
4	30 °	42.22	2245.2	113.11	-1222.8	-1401.9	
5	40 °	37.35	2123.3	23.51	-1420.4	-1028.5	
6	50°	31.34	1932.1	-30.54	-1451.1	-691.42	
7	60°	24.37	1679	-61.37	-1359.6	-409.17	
8	70°	16.67	1373.3	-75.05	-1179.1	-187.81	
9	80°	8.46	1025.6	-74.76	-934.65	-29.95	

The table 4.2 below shows x and y components of hydraulic forces on top blade i.e. at first stage and that on bottom blade i.e. at second stage, at different blade inlet angle keeping the other parameter same as designed, have been tabulated below.

Table 4.2 X and Y components of hydraulic forces at varying inlet blade angle

S.N.	β_1	Angular speed rad/s	$F_{xt}(N)$	$F_{yt}(N)$	$F_{xb}(N)$	$F_{yb}(N)$	Remark
1	0 °	44.5	2150	978.75	338.36	-2094.4	
2	10 °	44.5	2161.8	730.29	56.11	-2009.2	
3	20 °	44.5	2196.6	533.16	-270.23	-1935.4	
4	30 °	44.5	2253.6	375.13	-629.4	-1837	
5	40°	44.5	2334.4	246.04	-1006.9	-1690.8	
6	50 °	44.5	2447.2	137.22	-1393	-1486.3	
7	60 °	44.5	2617.6	39.97	-1797.4	-1222.6	
8	70 °	44.5	2930.4	-58.82	-2292.8	-899.59	
9	80°	44.5	3820.4	-205.24	-3305.6	-487.18	

4.5. Mathematical Model

The coordinate system of the runner of crossflow turbine runner which is shown in figure 4.2 as simply supported flexible beam with shaft and drum system, was defined according to z-axis in longitudinal direction towards right, y-axis along upwards vertical transverse direction and x-axis along the horizontal transverse direction perpendicular to both the y-axis and z-axis..

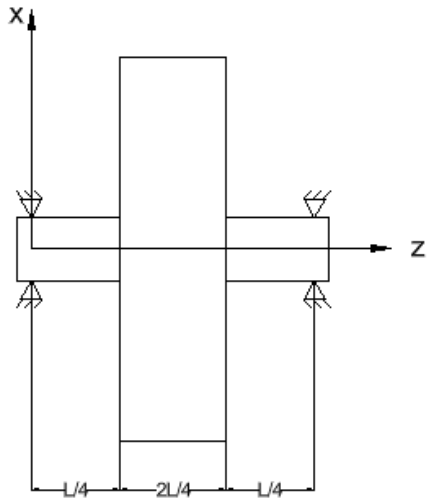

Figure 4.2 Shaft-Drum system symetic diagram

The displacements of any point of the shaft and drum along horizontal and vertical transverse directions are *u(z,t)* and *v(z,t)* respectively.

4.5.1. Kinematics of The Flexible Element

Let Ω is the angular velocity of the turbine runner.

In vector form,

$\overrightarrow{\omega}_s = \overrightarrow{\omega}_d = \Omega\,\overrightarrow{k}$

Where ω_s and ω_d are the angular velocity vector of the shaft and drum, respectively.

The position vector of any point about neutral axis is given as

$\overrightarrow{r_f} = u\,\overrightarrow{i} + v\,\overrightarrow{j}$

Then velocity vector of any point about neutral axis of the flexible element is

$\overrightarrow{V_f} = \overrightarrow{r_f} + \overrightarrow{\omega} * \overrightarrow{r_f}$

$\overrightarrow{V_f} = (\dot{u} - \ \Omega v)\ \overrightarrow{i} + (\dot{v} + \ \Omega u)\ \overrightarrow{j}$

Then, the Angular velocity vector of this flexible element is

$\overrightarrow{\omega_f} = \left(-\Omega v' + \dot{u}'\right)\ \overrightarrow{i} + \left(-\Omega u - \dot{v}'\right)\ \overrightarrow{j} + (\Omega + u'\ \dot{v}')\ \overrightarrow{k}$ (25)

So, the kinetic Energy of flexible shaft is

$KE_s = \frac{1}{2}\rho_s A_s \int_0^{L/4}[(\dot{u}-\Omega v)^2+(\dot{v}+\Omega u)^2]dz + \frac{1}{2}\rho_s J_s \int_0^{L/4}[(\Omega + u'\dot{v}')^2]dz +$
$\frac{1}{2}\rho_s I_s \int_0^{L/4}[(-\Omega u^{'}-\dot{v}')^2+(-\Omega v^{'}+\dot{u}')^2]dz+\frac{1}{2}\rho_s A_s \int_{3L/4}^{L}[(\dot{u}-\Omega v)^2+(\dot{v}+\Omega u)^2]dz+$
$\frac{1}{2}\rho_s J_s \int_{3L/4}^{L}[(\Omega + u'\dot{v}')^2]dz + \frac{1}{2}\rho_s I_s \int_{3L/4}^{L}[(-\Omega u^{'}-\dot{v}')^2+(-\Omega v^{'}+\dot{u}')^2]dz$

And the kinetic energy of flexible drum is

$KE_d = \frac{1}{2}\rho_d A_d \int_{L/4}^{3L/4}[(\dot{u}-\Omega v)^2+(\dot{v}+\Omega u)^2]dz + \frac{1}{2}\rho_d J_d \int_{L/4}^{3L/4}[(\Omega + u'\dot{v}')^2]dz +$
$\frac{1}{2}\rho_d I_d \int_{L/4}^{3L/4}[(-\Omega u^{'}-\dot{v}')^2+(-\Omega v^{'}+\dot{u}')^2]dz$

Total Kinetic Energy shaft and drum,

$KE = KE_s + KE_d$

Now, expanding and neglecting the higher order term,

$KE = \frac{1}{2}\rho_s A_s \int_0^{\frac{L}{4}} \dot{u}^2 dz + \frac{1}{2}\rho_s A_s \int_0^{\frac{L}{4}} \dot{v}^2 dz + \frac{1}{2}\rho_s A_s \Omega^2 \int_0^{\frac{L}{4}} u^2 dz + \frac{1}{2}\rho_s A_s \Omega^2 \int_0^{\frac{L}{4}5} v^2 dz +$
$\rho_s A_s \Omega \int_0^{\frac{L}{4}} \dot{v}udz - \rho_s A_s \Omega \int_0^{\frac{L}{4}} \dot{u}vdz + \frac{1}{2}\rho_s J_s \Omega^2 L/5 + \rho_s J_s \Omega \int_0^{\frac{L}{4}} \dot{v}^{'}u^{'}dz + \frac{1}{2}\rho_s I_s \int_0^{\frac{L}{4}} \dot{u}^{'2} dz +$
$\frac{1}{2}\rho_s I_s \int_0^{\frac{L}{4}} \dot{v}'^2 dz + \frac{1}{2}\rho_s I_s \Omega^2 \int_0^{\frac{L}{4}} u^{'2} dz + \frac{1}{2}\rho_s I_s \Omega^2 \int_0^{\frac{L}{4}} v^{'2} dz + \rho_s I_s \Omega \int_0^{\frac{L}{4}} \dot{v}^{'}u^{'}dz - \rho_s I_s \Omega \int_0^{\frac{L}{4}} \dot{u}^{'}v^{'}dz +$
$\frac{1}{2}\rho_d A_d \int_{\frac{L}{4}}^{\frac{3L}{4}} \dot{u}^2 dz + \frac{1}{2}\rho_d A_d \int_{\frac{L}{4}}^{\frac{3L}{4}} \dot{v}^2 dz + \frac{1}{2}\rho_d A_d \Omega^2 \int_{\frac{L}{4}}^{\frac{3L}{4}} u^2 dz + \frac{1}{2}\rho_d A_d \Omega^2 \int_{\frac{L}{4}}^{\frac{3L}{4}} v^2 dz + \rho_d A_d \Omega \int_{\frac{L}{4}}^{\frac{3L}{4}} \dot{v}udz -$
$\rho_d A_d \Omega \int_{\frac{L}{4}}^{\frac{3L}{4}} \dot{u}vdz + \frac{1}{2}\rho_d J_d \Omega^2 3L/5 + \rho_d J_d \Omega \int_{\frac{L}{4}}^{\frac{3L}{4}} \dot{v}^{'}u^{'}dz + \frac{1}{2}\rho_d I_d \int_{\frac{L}{4}}^{\frac{3L}{4}} \dot{u}^{'2} dz + \frac{1}{2}\rho_d I_d \int_{\frac{L}{4}}^{\frac{3L}{4}} \dot{v}'^2 dz +$
$\frac{1}{2}\rho_d I_d \Omega^2 \int_{\frac{L}{4}}^{\frac{3L}{4}} u^{'2} dz + \frac{1}{2}\rho_d I_d \Omega^2 \int_{\frac{L}{4}}^{\frac{3L}{4}} v^{'2} dz + \rho_d I_d \Omega \int_{\frac{L}{4}}^{\frac{3L}{4}} \dot{v}^{'}u^{'}dz - \rho_d I_d \Omega \int_{\frac{L}{5}}^{\frac{3L}{4}} \dot{u}^{'}v^{'}dz +$
$\frac{1}{2}\rho_s A_s \int_{\frac{3L}{4}}^{L} \dot{u}^2 dz + \frac{1}{2}\rho_s A_s \int_{\frac{3L}{4}}^{L} \dot{v}^2 dz + \frac{1}{2}\rho_s A_s \Omega^2 \int_{\frac{3L}{4}}^{L} u^2 dz + \frac{1}{2}\rho_s A_s \Omega^2 \int_{\frac{3L}{4}}^{L} v^2 dz + \rho_s A_s \Omega \int_{\frac{3L}{4}}^{L} \dot{v}udz -$
$\rho_s A_s \Omega \int_{\frac{3L}{4}}^{L} \dot{u}vdz + \frac{1}{2}\rho_s J_s \Omega^2 L/5 + \rho_s J_s \Omega \int_{\frac{3L}{4}}^{L} \dot{v}^{'}u^{'}dz + \frac{1}{2}\rho_s I_s \int_{\frac{3L}{4}}^{L} \dot{u}^{'2} dz + \frac{1}{2}\rho_s I_s \int_{\frac{3L}{4}}^{L} \dot{v}'^2 dz +$
$\frac{1}{2}\rho_s I_s \Omega^2 \int_{\frac{3L}{4}}^{L} u^{'2} dz + \frac{1}{2}\rho_s I_s \Omega^2 \int_{\frac{3L}{4}}^{L} v^{'2} dz + \rho_s I_s \Omega \int_{\frac{3L}{4}}^{L} \dot{v}^{'}u^{'}dz - \rho_s I_s \Omega \int_{\frac{3L}{4}}^{L} \dot{u}^{'}v^{'}dz$

The potential energy stored in shaft due to bending is then given by

$PE_s = \frac{1}{2}EI_s \int_0^{L/4}[(u'')^2+(v'')^2]dz + \frac{1}{2}EI_s \int_{\frac{3L}{4}}^{L}[(u'')^2+(v'')^2]dz$

The potential energy stored in flexible drum due to bending,

$PE_d = \frac{1}{2}EI_d \int_{L/4}^{\frac{3L}{4}}[(u'')^2+(v'')^2]dz$

Total potential energy

$PE = PE_s + PE_d$

$$PE = \frac{1}{2}EI_s \int_0^{L/4} [(u'')^2 + (v'')^2]dz + \frac{1}{2}EI_s \int_{\frac{3L}{4}}^{L} [(u'')^2 + (v'')^2]dz + \frac{1}{2}EI_d \int_{L/4}^{\frac{3L}{4}} [(u'')^2 + (v'')^2]dz$$

Work done due to hydraulic forces is given by

$W_{hydf} = [u\{F_{xt}(t) + F_{xb}(t)\} + v\{F_{yt}(t) + F_{yb}(t)\}] \mid_{\text{z=L/2}}$

4.5.2. Equation of Motion

The Lagrangian is given by

$\mathcal{L} = KE - PE$

Now, applying Hamilton's principle,

$\int_{t_1}^{t_2} (\delta\mathcal{L} + \delta W_{hydf})\, dt = 0$

By substituting the values of the total kinetic energy, potential energy and the working done by hydraulic force in the above equation and expanding, the equation of motion is achieved as systems of coupled differential equation with its associated boundary conditions.

4.6. Simulation Work

The geometry of crossflow turbine runner as shown in the figure 4.3 is modeled in autoCAD with the dimension obtained from design of the runner which is given in the table 4.3 and is imported as .IGES file to ANSYS for modal analysis and harmonic analysis.

Table 4.3 Modeling Parameters

S.N.	Parameters	Values
1	Outer Diameter	300 mm
2	Inner Diameter	204 mm
3	Runner width	83 mm

Table 4.3 Modeling Parameters

S.N.	Parameters	Values
4	Jet Thickness	48 mm
5	Nos. of Blade	23
6	Blade Thickness	5 mm
7	Radius of curvature of blade	52 mm

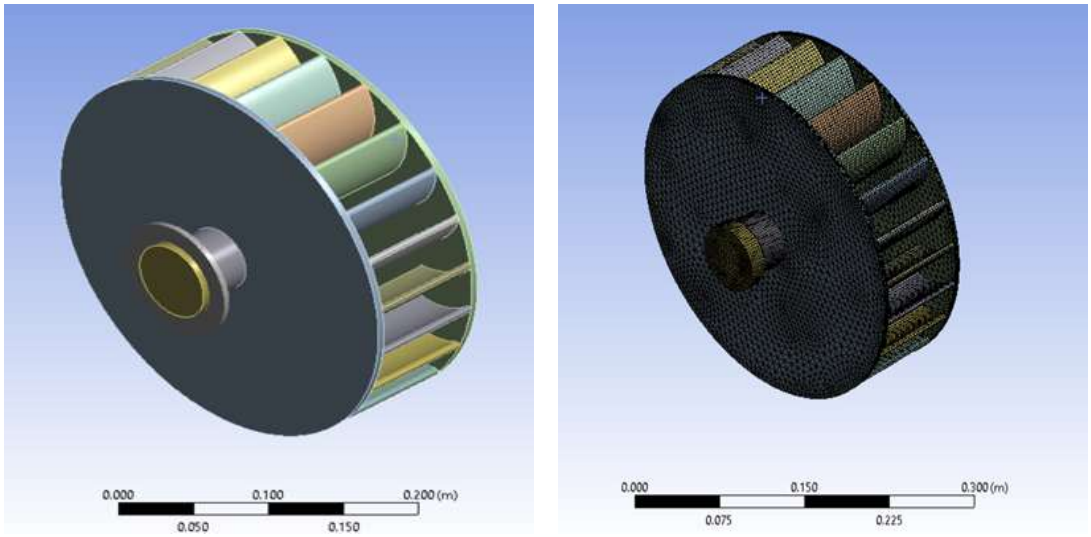

((a)) Runner geometry CAD model ((b)) Runner geometry with mesh

Figure 4.3 Plot of runner geometry and runner geomerty with mesh

CHAPTER FIVE: RESULTS AND DISCUSSION

5.1. Expression of Governing Equation and Associated Boundary condition

The governing equation for motion of the crossflow turbine runner is achieved as coupled differential equation with its associated boundary conditions.

For shaft element, $0 \leq z \leq L/4$

$$\rho_s A_s \ddot{u} - 2\rho_s A_s \Omega \dot{v} - \rho_s A_s \Omega^2 u + \rho_s J_s \Omega \dot{v}'' + 2\rho_s I_s \Omega \dot{v}'' - \rho_s I_s \ddot{u}'' + \rho_s I_s \Omega^2 u'' + EI_s u^{IV} = 0$$

$$\rho_s A_s \ddot{v} - 2\rho_s A_s \Omega \dot{u} - \rho_s A_s \Omega^2 v + \rho_s J_s \Omega \dot{u}'' + 2\rho_s I_s \Omega \dot{u}'' - \rho_s I_s \ddot{v}'' + \rho_s I_s \Omega^2 v'' + EI_s v^{IV} = 0$$

For drum element, $L/4 \leq z \leq 3L/4$

$$\rho_d A_d \ddot{u} - 2\rho_d A_d \Omega \dot{v} - \rho_d A_d \Omega^2 u + \rho_d J_d \Omega \dot{v}'' + 2\rho_d I_d \Omega \dot{v}'' - \rho_d I_d \ddot{u}'' + \rho_d I_d \Omega^2 u'' + EI_d u^{IV} = \delta\left(z - \tfrac{L}{2}\right).\{F_{xt}(t) + F_{xb}(t)\}$$

$$\rho_d A_d \ddot{v} - 2\rho_d A_d \Omega \dot{u} - \rho_d A_d \Omega^2 v + \rho_d J_d \Omega \dot{u}'' + 2\rho_d I_d \Omega \dot{u}'' - \rho_d I_d \ddot{v}'' + \rho_d I_d \Omega^2 v'' + EI_d v^{IV}$$

$$= \delta\left(z - \tfrac{L}{2}\right).\{F_{yt}(t) + F_{yb}(t)\}$$ For shaft element, $3L/4 \leq z \leq L$

$$\rho_s A_s \ddot{u} - 2\rho_s A_s \Omega \dot{v} - \rho_s A_s \Omega^2 u + \rho_s J_s \Omega \dot{v}'' + 2\rho_s I_s \Omega \dot{v}'' - \rho_s I_s \ddot{u}'' + \rho_s I_s \Omega^2 u'' + EI_s u^{IV} = 0$$

$$\rho_s A_s \ddot{v} - 2\rho_s A_s \Omega \dot{u} - \rho_s A_s \Omega^2 v + \rho_s J_s \Omega \dot{u}'' + 2\rho_s I_s \Omega \dot{u}'' - \rho_s I_s \ddot{v}'' + \rho_s I_s \Omega^2 v'' + EI_s v^{IV} = 0$$

The associated boundary conditions are,

at $z = 0$

$u(0,t) = 0$ $v(0,t) = 0$ (Displacement boundary condition)

$u'(0,t) = 0$ $v'(0,t) = 0$ (Slope boundary condition)

at $z = L/4$

$u_s(L/4,t) = u_d(L/4,t)$ $v_s(L/4,t) = v_d(L/4,t)$ (Continuity of displacement)

$u'_s(L/4,t) = u'_d(L/4,t)$ $v'_s(L/4,t) = v'_d(L/4,t)$ (Continuity of slope)

$E_s I_s u''(L/4,t) = E_d I_d u''(L/4,t)$ $E_s I_s v''(L/4,t) = E_d I_d v''(L/4,t)$ (Bending Moment continuity)

$E_s I_s u'''(L/4,t) = E_d I_d u'''(L/4,t)$ $E_s I_s v'''(L/4,t) = E_d I_d v'''(L/4,t)$ (Shear force continuity)

at $z = 4L/5$

$u_s(3L/4,t) = u_d(3L/4,t)$ $v_s(3L/4,t) = v_d(3L/4,t)$ (Continuity of displacement)

$u'_s(3L/4,t) = u'_d(3L/4,t)$ $v'_s(3L/4,t) = v'_d(3L/4,t)$ (Continuity of slope)

$E_s I_s u''(3L/4,t) = E_d I_d u''(3L/4,t)$ $E_s I_s v''(3L/4,t) = E_d I_d v''(3L/4,t)$

(Bending Moment continuity)

$E_s I_s u'''(L/4,t) = E_d I_d u'''(L/4,t)$ $E_s I_s v'''(L/4,t) = E_d I_d v'''(L/4,t)$ (Shear force continuity)

$u_s(3L/4,t) = u_s(L/4,t)$ $v_s(3L/4,t) = v_s(L/4,t)$ (Symmetry of displacement)

$u'_s(3L/4,t) = u'_s(L/4,t)$ $v'_s(3L/4,t) = v'_s(L/4,t)$ (Symmetry of slope)

At $z = L$

$u(L,t) = 0$ $v(L,t) = 0$ (Displacement boundary condition)

$u'(L,t) = 0$ $v'(L,t) = 0$ (Slope boundary condition)

The governing equation of motion effectively models the dynamic behavior of the crossflow turbine runner, incorporating inertia effects, gyroscopic effects, Coriolis forces, and bending stiffness. The system is segmented into shaft and drum elements with continuity enforced at the interfaces. The boundary conditions ensure realistic physical behavior, including displacement, slope, moment, and shear force continuity, while symmetry conditions simplify the model. The hydraulic force components are applied at mid-span using a Dirac delta function.

5.2. Campbell Diagram and Critical Speed

The Campbell Diagram of modal analysis for applied spin speed steps 0 rad/s, 44.5 rad/s and 100 rad/s is shown in figure 5.1 below. The only one critical speed

is found to be 7.33×10^{-3} rad/s. The Campbell Diagram as shown in the figure 5.3 for applied spin speed range from 1000 rad/s to 10000 rad/s show eight critical speeds; which are1386.5 rad/s, 1913 rad/s, 2136.5 rad/s, 2286.4 rad/s, 3385.4 rad/s, 4832.5 rad/s, 5741.1 rad/s and 8743.2 rad/s. No critical speed is found in the spin speed range between the range 100 rad/s to 1000 rad/s; the Campbell, diagram is shown in the figure 5.2.

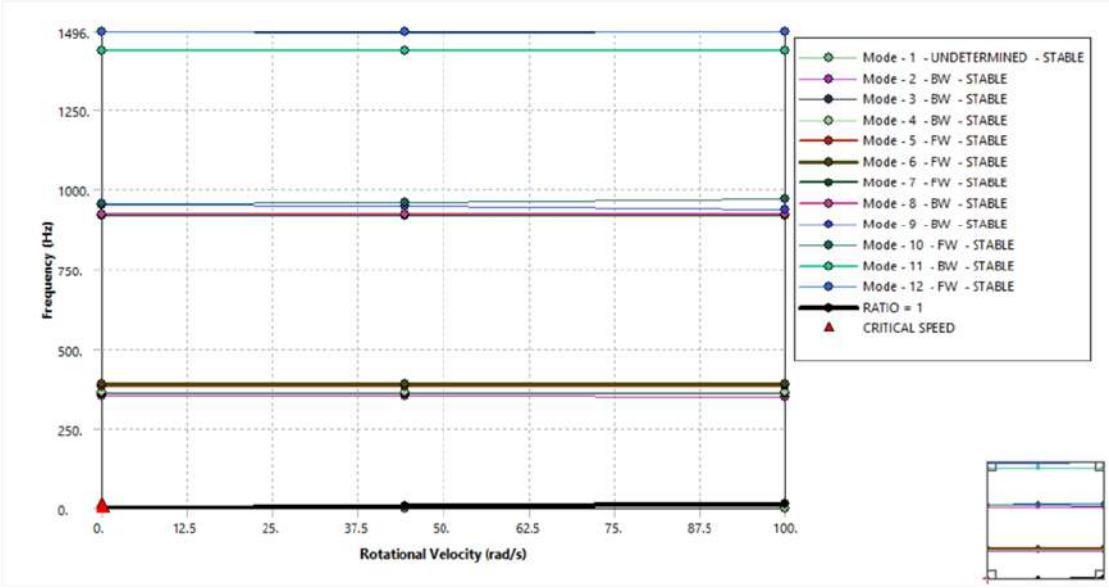

Figure 5.1 Campbell diagram for the spin speed steps 0 rad/s, 44.5 rad/s and 100 rad/s

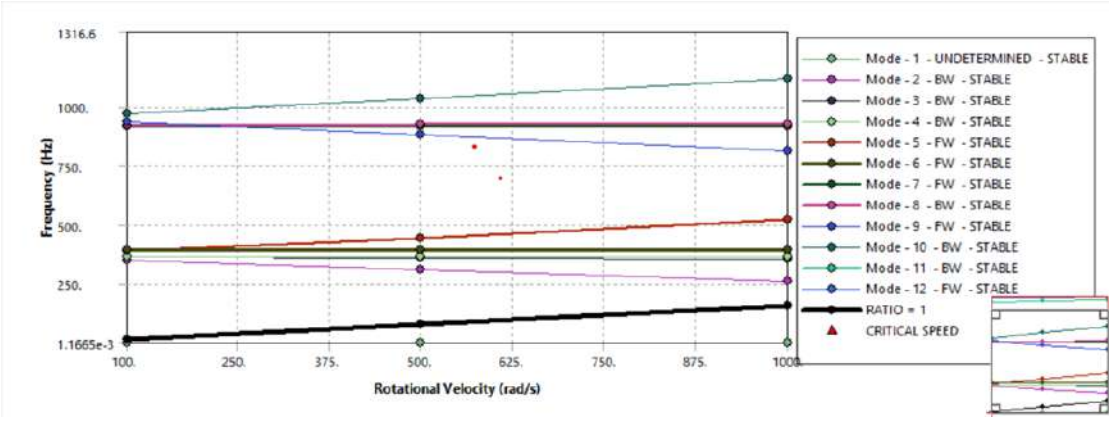

Figure 5.2 Campbell Diagram for spin speed range from 100 rad/s to 1000 rad/s

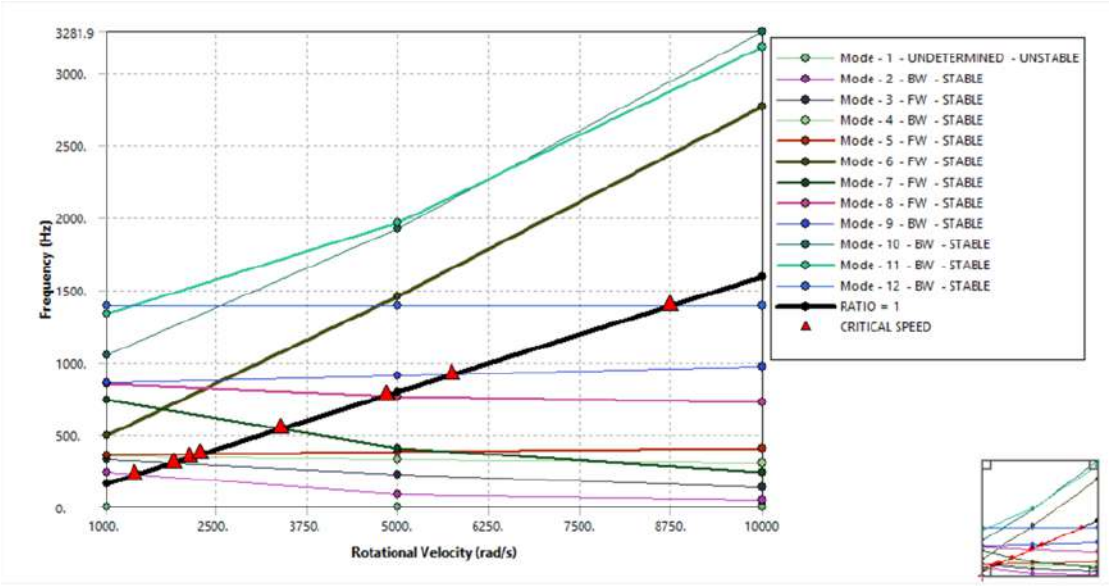

Figure 5.3 Campbell Diagram for spin speed range from 1000 rad/s to 10000 rad/s

5.3. Major Mode Shapes and Natural Frequencies

The figures 5.4, 5.5, 5.6 and 5.7 show four major mode shapes out of twelve modes, which are for minimum natural frequency, for maximum natural frequency, for highest maximum deformation and for maximum deformation at shaft-disc joint of the crossflow turbine runner.

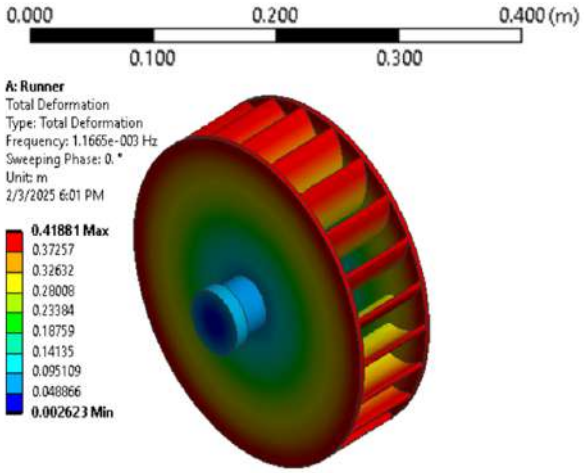

Figure 5.4 This is the first mode of first point of spin speed steps 0 rad/s, 44.5 rad/s and 100 rad/s and this mode has minimum natural frequency of 1.665×10^{-3} Hz

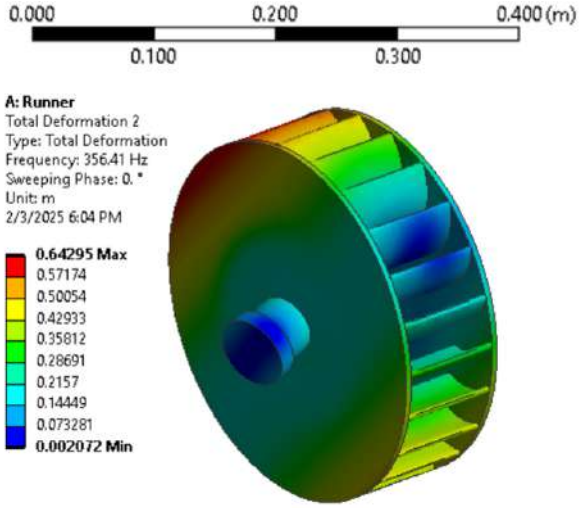

Figure 5.5 This is the second mode of first point of spin speed steps 0 rad/s, 44.5 rad/s and 100 rad/s and this mode has highest max. deformation and the natural frequency of 356.41 Hz.

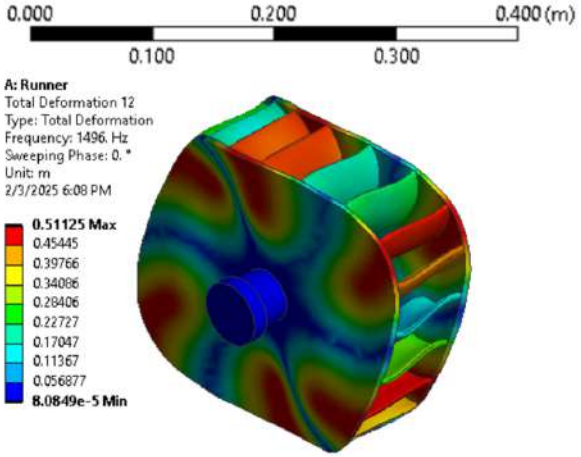

Figure 5.6 This is the last mode of first point of spin speed steps 0 rad/s, 44.5 rad/s and 100 rad/s and this mode has maximum natural frequency of 1496 Hz

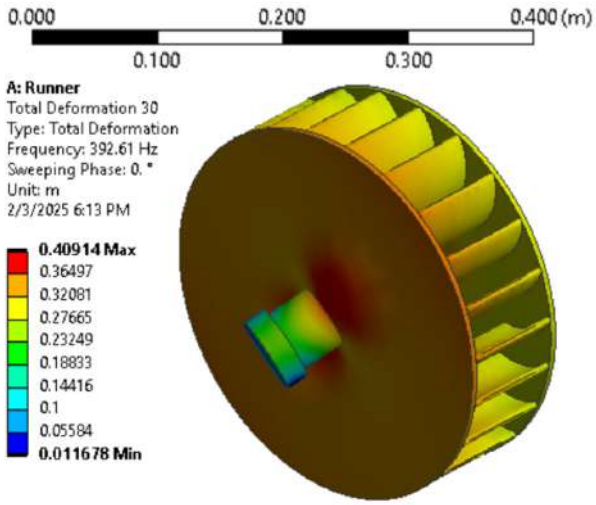

Figure 5.7 This is the sixth mode of third point of spin speed steps 0 rad/s, 44.5 rad/s and 100 rad/s and this mode shows highest deformation at shaft-disc joint and has natural frequency 392.61 Hz

These mode shapes help identify key vibrations and potential structural weak-

ness, particularly at the shaft-disc interface, which may be essential for design optimization and ensuring dynamic stability.

5.4. Frequency Response of Harmonic Analysis

The frequency response from harmonic analysis provided the maximum amplitudes in the x-direction and y-direction for various force vectors caused by changes in the inlet blade and angle angle of attack. These values are presented in table 5.1 and table 5.2 respectively, which indicate that the amplitude in the y-direction is consistently higher than in the x-direction for all angles of attack and inlet blade angles. Furthermore, the table reveals that vibration amplitude increases with increase in the inlet blade angle. However, for the angle of attack, the amplitude initially rises up to 20° before decreasing with further increases in the angle of attack.

Table 5.1 X and Y components of hydraulic forces at varying inlet blade angle

S.N.	Beta	Amaxx (m)	Amaxy (m)
1	0 °	3.998×10^{-4}	1.294×10^{-3}
2	10 °	4.045×10^{-4}	1.335×10^{-3}
3	20 °	4.16×10^{-4}	1.39×10^{-3}
4	30 °	4.272×10^{-4}	1.448×10^{-3}
5	40°	4.37×10^{-4}	1.449×10^{-3}
6	50 °	4.452×10^{-4}	1.542×10^{-3}
7	60 °	4.551×10^{-4}	1.588×10^{-3}
8	70 °	4.786×10^{-4}	1.68×10^{-3}
9	80°	5.759×10^{-4}	2.029×10^{-3}

Table 5.2 X and Y components of hydraulic forces at varying attack angle

S.N.	Alpha	Amaxx (m)	Amaxy (m)
1	0 °	4.172×10^{-4}	1.347×10^{-3}
2	10 °	4.314×10^{-4}	1.437×10^{-3}
3	20 °	4.309×10^{-4}	1.468×10^{-3}
4	30 °	4.104×10^{-4}	1.419×10^{-3}
5	40°	3.714×10^{-4}	1.294×10^{-3}
6	50 °	3.222×10^{-4}	1.129×10^{-3}
7	60 °	2.668×10^{-4}	9.379×10^{-4}
8	70 °	2.078×10^{-4}	7.323×10^{-4}
9	80°	1.475×10^{-4}	5.214×10^{-4}

where Beta is inlet blade angle, Alfa is angle of attack, Amaxx is the maximum amplitude in x direction and Amaxy is the maximum amplitude in y direction.

The plot showing variation in maximum amplitudes in x-direction and y-direction versus variation in inlet blade angle are presented in figure 5.8 and 5.9 while corresponding variations versus angle of attack are presented in the figures 5.10 and 5.11.

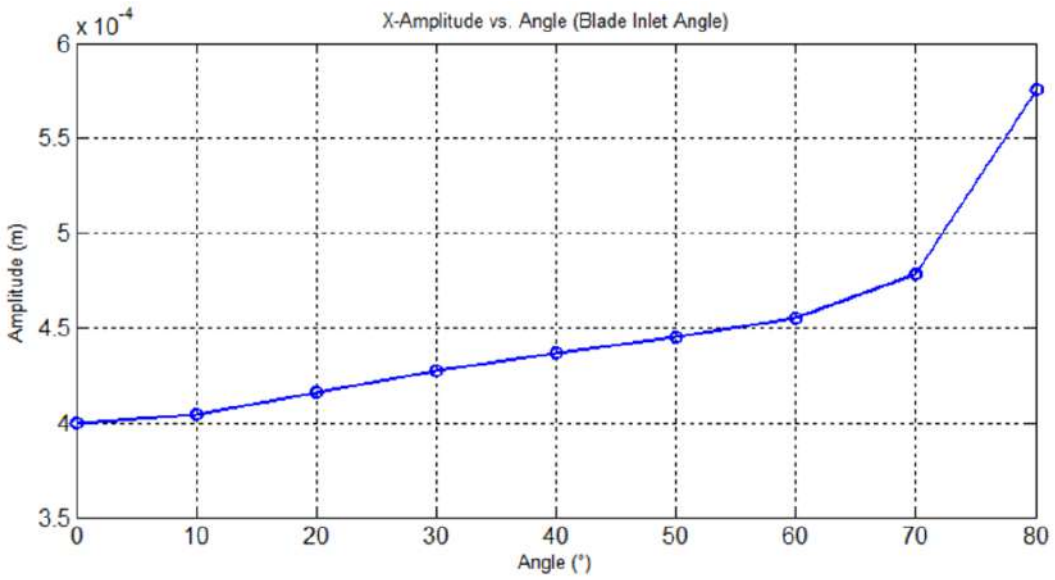

Figure 5.8 Max. Amplitude in x-direction vs. Inlet Blade Angle

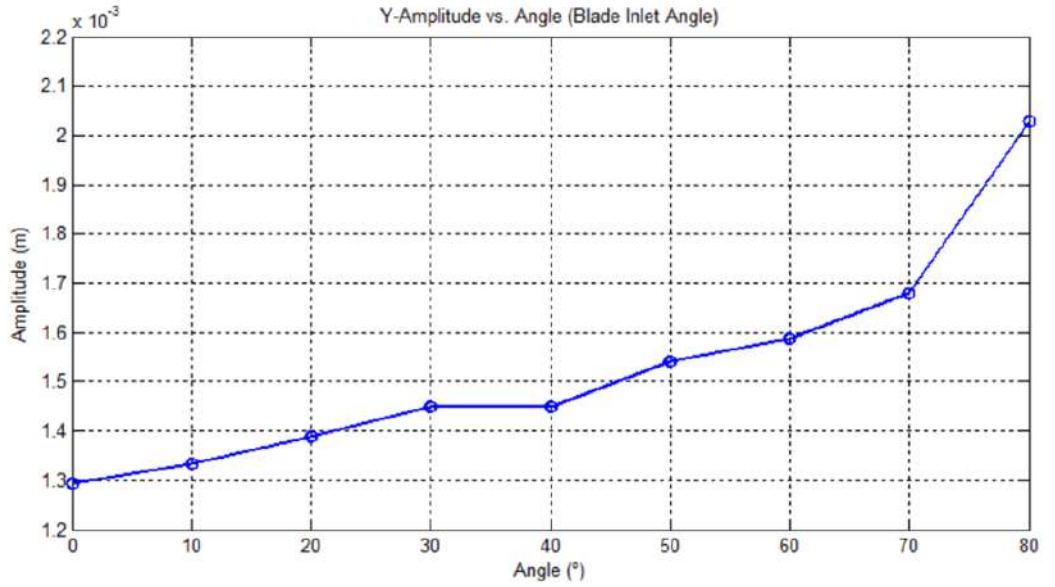

Figure 5.9 Max. Amplitude in y-direction vs. Inlet Blade Angle

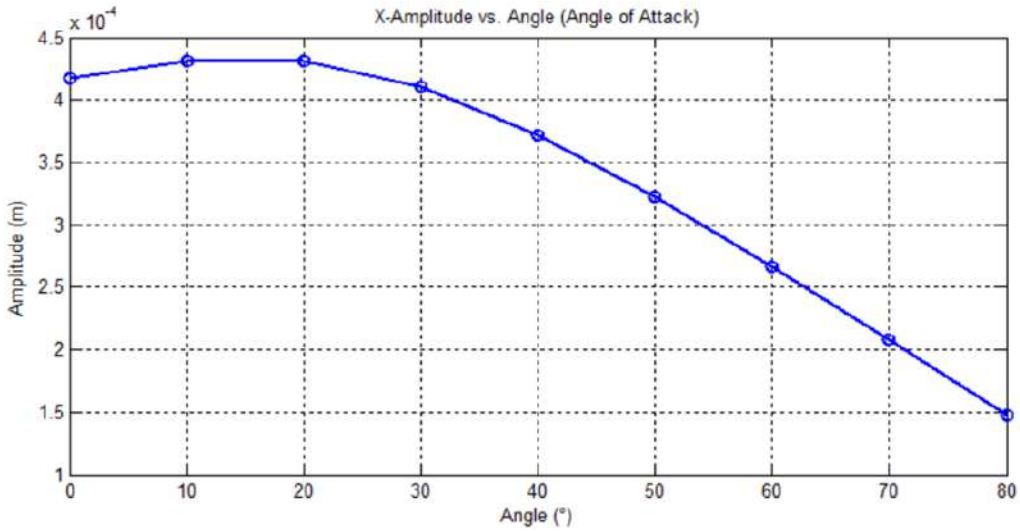

Figure 5.10 Max. Amplitude in x-direction vs. Angle of Attack

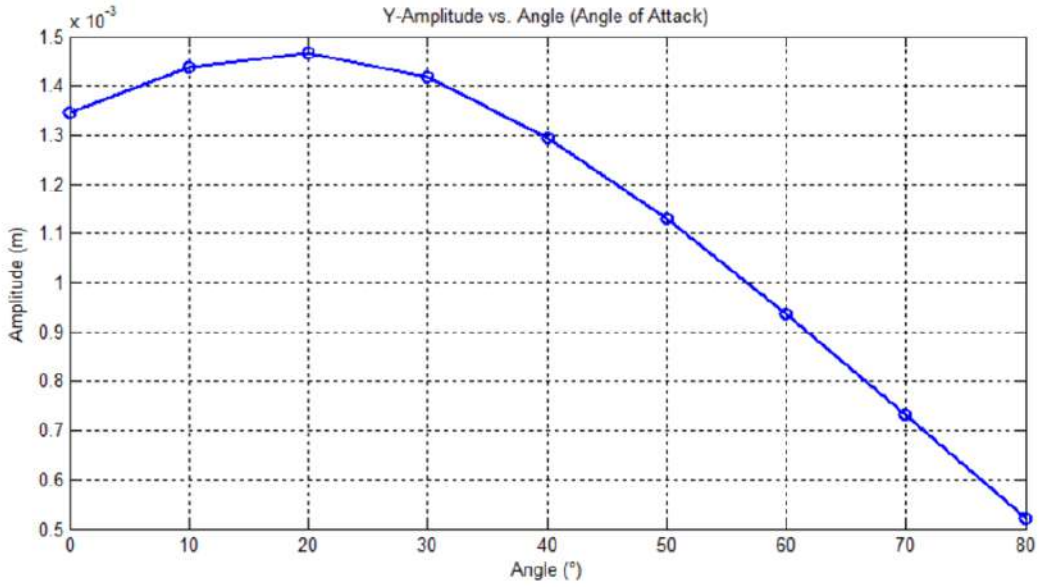

Figure 5.11 Max. Amplitude in y-direction vs. Angle of Attack

The graphs in Figures 5.8 and 5.9 depict the maximum amplitudes in the x-direction and y-direction obtained from the frequency response of harmonic analysis for various force vectors. These amplitudes increase with the increment in the blade angle at the inlet. In contrast, Figures 5.10 and 5.11 show an increase in the angle of attack leads to a rise in maximum amplitude up to 20°, after which it begins to decrease in both the x-direction and y-direction.

From these graphs, it can be inferred that an increase in the inlet blade angle may amplify the water impact force, resulting in higher vibration amplitudes in both the x and y directions. Likewise, as the angle of attack increases up to 20°, the water impact force may intensify, leading to greater amplitude. However, beyond 20°, flow separation and turbulence may occur, reducing effective force transfer and causing a decline in vibration amplitudes. Additionally, structural damping and resonance effects could also contribute to this behavior.

CHAPTER SIX: CONCLUSION AND RECOMMENDATION

6.1. Conclusion

The crossflow turbine runner is systematically designed based on the given gross head and flow rate, ensuring optimal geometry for modal analysis.

The force vectors that act on the runner's blades are analyzed using velocity triangles for varying angles of attack and inlet blade angles. This analysis provided essential input for the harmonic analysis.

The governing equation of motion of the crossflow turbine runner with its associated boundary condition is obtained by applying Hamilton's principle assuming the turbine runner shaft-drum combination as flexible member and Euler-Bernoulli beam model.

The first critical speed is 7.33×10^{-3} rad/s, making the system susceptible to resonance conditions during startup and shutdown. As a result, the crossflow turbine runner may experience high-amplitude vibrations, potentially leading to instability during these phases of operation. Enhancing damping mechanisms, optimizing bearing support stiffness, and adjusting operational procedures can minimize resonance effects and improve stability. Since the other critical speeds are well beyond the operating speed range, the system can operate stably with a minimal risk of resonance and high-amplitude vibrations at operating speed.

The interpretation of the graphs from the results provides valuable insights for optimizing the inlet blade angle and angle of attack. By adjusting these parameters, it is possible to minimize the vibration response of the crossflow turbine runner. This optimization can lead to enhanced operational stability, reduced mechanical stress and reliable turbine operation.

6.2. Recommendation

In this study, the design of the crossflow turbine runner has been completed, the governing equation of motion of the runner has been obtained, modal analysis has been conducted, and the harmonic analysis has been performed for varying force vectors. Although these analyses offer valuable information, more work is needed to enhance the findings. The following recommendations are made for future efforts:

- Solving the Governing Equation of Motion.
- Conducting Experimental test for Validation of simulation work.
- Analysis can be done for varying jet width.

REFERENCES

[1] M. Tiwari and R. Shrestha, "Effect of variation of design parameters on cross flow turbine efficiency using ansys," *Journal of the Institute of Engineering*, vol. 13, no. 1, pp. 1–9, 2017.

[2] J. Butchers, *Enabling sustainable and reliable energy using locally manufactured micro-hydropower technology.* PhD thesis, University of Bristol, 2021.

[3] L. Motra and M. C. Luintel, "Free vibration analysis of selected pelton turbine using dynamic approach," in *Proceedings of IOE Graduate Conference*, vol. 5, pp. 229–236, 2017.

[4] C. Mockmore, "The banki water turbine," *Engineering Experiment Station, Oregon State System of Higher Education, Oregon State College*, 1949.

[5] J. Šašek, M. Hajžman, and V. Zeman, "Modelling of rotating shafts with flexible disks," in *PAMM: Proceedings in Applied Mathematics and Mechanics*, vol. 7, pp. 4050007–4050008, Wiley Online Library, 2007.

[6] N. Khader, A. Atoum, and A. Al-Qaisia, "Theoretical and experimental modal analysis of multiple flexible disk-flexible shaft system," in *SEM annual Conference, Springfield, Massachusetts*, 2007.

[7] Y.-D. Choi, J.-I. Lim, Y.-T. Kim, and Y.-H. Lee, "Effect of blade angle on the performance of a cross-flow hydro turbine," *Journal of Advanced Marine Engineering and Technology*, vol. 32, no. 3, pp. 413–420, 2008.

[8] D. Srikrishnanivas, "Rotor dynamic analysis of rm12 jet engine rotor using ansys," 2012.

[9] W. Shi, C.-W. Kim, C.-W. Chung, and H.-C. Park, "Dynamic modeling and analysis of a wind turbine drivetrain using the torsional dynamic model," *International journal of precision engineering and manufacturing*, vol. 14, pp. 153–159, 2013.

[10] X. Huang, E. Egusquiza, C. Valero, and A. Presas, "Dynamic behaviour of pump-turbine runner: From disk to prototype runner," in *IOP Conference Series: Materials Science and Engineering*, vol. 52, p. 022036, IOP Publishing, 2013.

[11] M. A. Khan and S. Badshah, "Research article design and analysis of cross flow turbine for micro hydro power application using sewerage water," *Res. J. Appl. Sci. Eng. Technol*, vol. 8, no. 7, pp. 821–828, 2014.

[12] S. Mirtalaie and M. Hajabasi, "A new methodology for modeling and free vibrations analysis of rotating shaft based on the timoshenko beam theory," *Journal of Vibration and Acoustics*, vol. 138, no. 2, p. 021012, 2016.

[13] R. Warjito, A. Siswantara, D. Adanta, A. Prakoso, and R. Dianofitra, "Comparison between airfoil naca-6712 profiled and ordinary blade in cross-flow turbine by numerical simulation," in *The 15th International Conference on Quality in Research (QiR 2017). Available at: https://scholar. ui. ac. id/en/publications/comparison-between-airfoil-naca-6712-profiled-and-ordinary-blade*, 2017.

[14] M. Luintel, *Dynamic modelling and response of a pelton turbine unit*. PhD thesis, Ph. D. Thesis, Lalitpur, Nepal, 2019.

[15] M. K. Al-Solihat and K. Behdinan, "Force transmissibility and frequency response of a flexible shaft–disk rotor supported by a nonlinear suspension system," *International Journal of Non-Linear Mechanics*, vol. 124, p. 103501, 2020.

[16] R. Koirala and M. C. Luitel, "Dynamic response of vertical shaft pelton turbine unit for forced vibration," *Journal of Innovations in Engineering Education*, vol. 4, no. 1, pp. 34–41, 2021.

[17] M. Zhang and Q.-G. Chen, "Numerical model on the dynamic behavior of a prototype kaplan turbine runner," *Mathematical Problems in Engineering*, vol. 2021, no. 1, p. 4421340, 2021.

[18] B. Pandey, "Vibration analysis of cantilever shaft-disk system for transient response to impact jet," 2023.

[19] M. Baral, K. Pokharel, and M. C. Luintel, "Transverse vibration analysis of hydro-generator assembly," 2023.

[20] Kelly, *Mechanical vibrations: theory and applications*. Cengage learning, 2012.

[21] T. Chandran, P. Surendran, and J. Chandapillai, "Design methodology and structural analysis of crossflow türbine," *Innovative Solutions in Flow Measurement and Control-Oil, WaterandGas" August28-30*, 2017.

[22] E. Quaranta, J. P. Perrier, and R. Revelli, "Optimal design process of cross-flow banki turbines: Literature review and novel expeditious equations," *Ocean Engineering*, vol. 257, p. 111582, 2022.

[23] N. B. Mereke, "Highly efficient cross flow turbine runner design for upgrading traditional water mill in to micro hydro power plant," *International Journalof Engineeering Research & Technology (IJERT)*, vol. 4, p. 12, 2015.

[24] A. Arter and U. Meier, *Harnessing Water Power on a Small Scale: Hydrolics Engineering Manual*. Swiss Centre for Appropriate Technology, 1990.

[25] H. Khanlo, M. Ghayour, and S. Ziaei-Rad, "Chaotic vibration analysis of rotating, flexible, continuous shaft-disk system with a rub-impact between the disk and the stator," *Communications in Nonlinear Science and Numerical Simulation*, vol. 16, no. 1, pp. 566–582, 2011.

APPENDIX: A

MATLAB Program to calculate force vector at various angle of attack

```
%clc
%clear all
N=850;% RPM
Do=0.3;% Outer dia.
Di=0.204; %inner dia
HN=45.421;% Net Head
Q=0.116;% designed flow rate
rho=1000;% density of water
V1=0.98*sqrt(2*9.81*HN);
clc;
all clear;
actang='enter the value of angle of attact';
alfa1=input(actang);
U1=0.5*V1*cosd(alfa1);
beta1=atand(2*tand(alfa1))
W1=(V1*cosd(alfa1)-U1)/cosd(beta1);
U2=U1*Di/Do;
W2=sqrt(W1.^2-U1.^2+U2.^2);
alfa2=atand(W2/U2);
V2=sqrt(W2.^2+U2.^2);
gama=((1-Di/Do)*U1*360)./(V2*2*pi);
beta2=90;
phy=11;
psy=gama+phy;
U3=U2; V3=V2; alfa3=alfa2;
W3=sqrt(V3.^2-U3.^2);
beta4=180-beta1;
U4=U1;W4=W1;
V4=sqrt(W4.^2+U4.^2+2*W4*U4*cosd(beta4));
alfa4=acosd((U1-W1*cosd(beta1))/V4);
theta1=beta1;
theta2=psy+90;
theta3=(2*alfa2+psy)-90;
theta4=2*alfa2+psy-phy-beta4;
fxt=rho*Q*(W1*cosd(theta1)-W2*cosd(theta2))
fyt=rho*Q*(W1*sind(theta1)-W2*sind(theta2))
ft=sqrt(fxt.^2+fyt.^2);
thetat=atand(fyt/fxt);
fxb=rho*Q*(W3*cosd(theta3)-W4*cosd(theta4))
fyb=rho*Q*(W3*sind(theta3)-W4*sind(theta4))
fb=sqrt(fxb.^2+fyb.^2);
thetab=atand(fyb/fxb);
p=pi*N*(ft+fb)*(Do+Di)/60;
```

MATLAB Program to calculate force vector at various inlet blade angle

```
clc
clear all
N=850;% RPM
Do=0.3;% Outer dia.
Di=0.204; %inner dia
HN=45.421;% Net Head
Q=0.116;% designed flow rate
rho=1000;% density of water
U1=pi*N*Do/60;
V1=0.98*sqrt(2*9.81*HN);
actang='enter the value of angle of attact';
alfa1=input(actang);
omega=U1/Do
beta1='enter the value of angle of blade at inlet';
beta1=input(beta1);
W1=(V1*cosd(alfa1)-U1)/cosd(beta1);
U2=U1*Di/Do;
W2=sqrt(W1.^2-U1.^2+U2.^2);
alfa2=atand(W2/U2);
V2=sqrt(W2.^2+U2.^2);
gama=((1-Di/Do)*U1*360)./(V2*2*pi);
beta2=90;
phy=11;
psy=gama+phy;
U3=U2; V3=V2; alfa3=alfa2;
W3=sqrt(V3.^2-U3.^2);
beta4=180-beta1;
U4=U1;W4=W1;
V4=sqrt(W4.^2+U4.^2+2*W4*U4*cosd(beta4));
alfa4=acosd((U1-W1*cosd(beta1))/V4);
theta1=beta1;
theta2=psy+90;
theta3=(2*alfa2+psy)-90;
theta4=2*alfa2+psy-phy-beta4;
fxt=rho*Q*(W1*cosd(theta1)-W2*cosd(theta2))
fyt=rho*Q*(W1*sind(theta1)-W2*sind(theta2))
ft=sqrt(fxt.^2+fyt.^2);
thetat=atand(fyt/fxt);
fxb=rho*Q*(W3*cosd(theta3)-W4*cosd(theta4))
fyb=rho*Q*(W3*sind(theta3)-W4*sind(theta4))
fb=sqrt(fxb.^2+fyb.^2);
thetab=atand(fyb/fxb);
p=pi*N*(ft+fb)*(Do+Di)/60;
```

MATLAB Program plot amplitude vs. various inlet blade angle and angle of attack

```
%plot for max. Amplitudes vs. angle of attack and inlet blade angle
% X-amplitude for varying Blade inlet angle
x1 = [3.998e-4, 4.045e-4, 4.16e-4, 4.272e-4, 4.37e-4, 4.452e-4,
4.551e-4, 4.786e-4, 5.759e-4];
y1 = [0, 10, 20, 30, 40, 50, 60, 70, 80];
% X-amplitude for varying angle of Attack
x2 = [4.172e-4, 4.314e-4, 4.309e-4, 4.104e-4, 3.714e-4, 3.222e-4,
2.668e-4, 2.078e-4, 1.475e-4];
y2 = [0, 10, 20, 30, 40, 50, 60, 70, 80];
% Y-amplitude for varying Blade inlet angle
x3 = [1.294e-3, 1.335e-3, 1.39e-3, 1.448e-3, 1.449e-3, 1.542e-3,
1.588e-3, 1.68e-3, 2.029e-3];
y3 = [0, 10, 20, 30, 40, 50, 60, 70, 80];
% Y-amplitude for varying angle of Attack
x4 = [1.347e-3, 1.437e-3, 1.468e-3, 1.419e-3, 1.294e-3, 1.129e-3,
9.379e-4, 7.323e-4, 5.214e-4];
y4 = [0, 10, 20, 30, 40, 50, 60, 70, 80];
% Plot 1: X-amplitude vs. Angle for Blade Inlet Angle
figure;
plot(y1, x1, 'b-o', 'LineWidth', 1.5, 'MarkerSize', 6);
xlabel('Angle (°)');
ylabel('Amplitude (m)');
title('X-Amplitude vs. Angle (Blade Inlet Angle)');
grid on;
% Plot 2: X-amplitude vs. Angle for Angle of Attack
figure;
plot(y2, x2, 'b-o', 'LineWidth', 1.5, 'MarkerSize', 6);
xlabel('Angle (°)');
ylabel('Amplitude (m)');
title('X-Amplitude vs. Angle (Angle of Attack)');
grid on;
% Plot 3: Y-amplitude vs. Angle for Blade Inlet Angle
figure;
plot(y3, x3, 'b-o', 'LineWidth', 1.5, 'MarkerSize', 6);
xlabel('Angle (°)');
ylabel('Amplitude (m)');
title('Y-Amplitude vs. Angle (Blade Inlet Angle)');
grid on;
% Plot 4: Y-amplitude vs. Angle for Angle of Attack
figure;
plot(y4, x4, 'b-o', 'LineWidth', 1.5, 'MarkerSize', 6);
xlabel('Angle (°)');
ylabel('Amplitude (m)');
title('Y-Amplitude vs. Angle (Angle of Attack)');
grid on;
```

APPENDIX: B

Assessment of Turbine Parameters

Mini-Grid Rural Electrification Component (MGREC)

MGREC Serial Number: 0284/ II

MGREC I.D.: 0572BAJ10SEP

Assessment of Turbine Parameters:

Name of the project:	**Rauda Gad MHP**	
Location	Dahakot VDC, Bajura	
Design flow:	116 lps	
Gross head	47 m	
RPM	850	
Penstock	Type	MS Flange Type
Transmission	Total Length	71.5 m
	ID of the pipe	**250 mm**
	Thickness	3.5 mm
Design Plant capacity	**30.5 kW**	
Installation Company	KP Byawasayi Sewa JV Synergy Company P L	
Manufacturing Company	Lumbini Engineering & Hydropower	
Turbine Type:	Cross Flow T-15	

APPENDIX: C

Email of acceptance for publication in IOEGC16

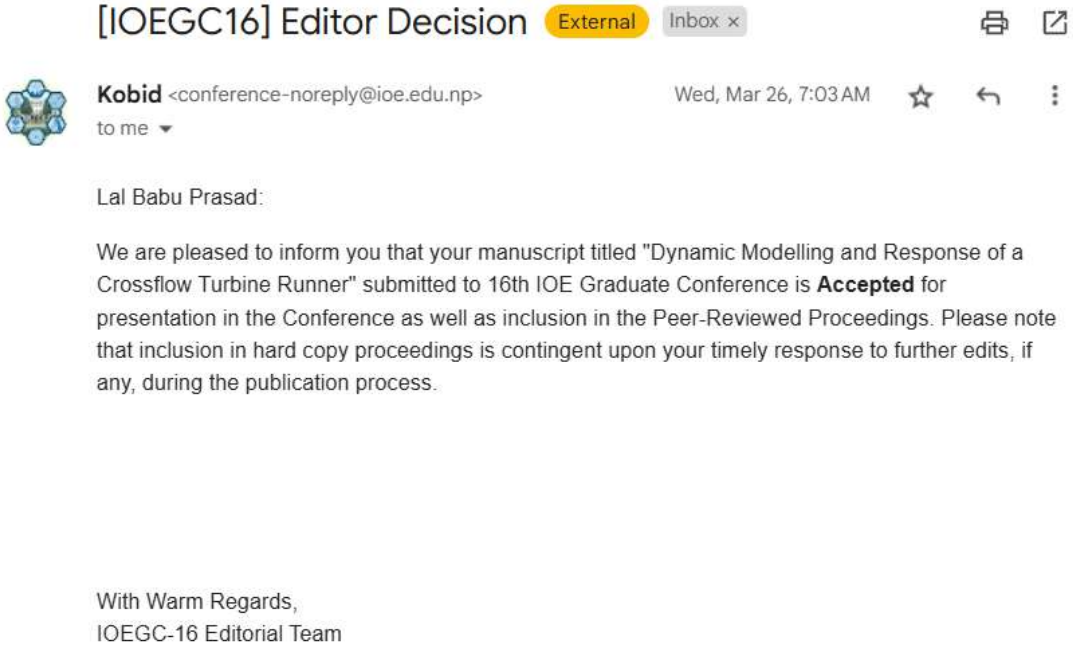

[IOEGC16] Editor Decision External Inbox ×

Kobid <conference-noreply@ioe.edu.np> Wed, Mar 26, 7:03 AM

to me

Lal Babu Prasad:

We are pleased to inform you that your manuscript titled "Dynamic Modelling and Response of a Crossflow Turbine Runner" submitted to 16th IOE Graduate Conference is **Accepted** for presentation in the Conference as well as inclusion in the Peer-Reviewed Proceedings. Please note that inclusion in hard copy proceedings is contingent upon your timely response to further edits, if any, during the publication process.

With Warm Regards,
IOEGC-16 Editorial Team

Plagiarism Report Certificate

Lal Babu Prasad

76msde012 (2).pdf

Tribhuvan University

Document Details

Submission ID
trn:oid:::3117:447278276

Submission Date
Apr 9, 2025, 4:07 PM GMT+5:45

Download Date
Apr 9, 2025, 4:10 PM GMT+5:45

File Name
76msde012 (2).pdf

File Size
2.8 MB

58 Pages

11,550 Words

59,570 Characters

iThenticate Page 1 of 66 - Cover Page Submission ID trn:oid:::3117:447278276

11% Overall Similarity

The combined total of all matches, including overlapping sources, for each database.

Filtered from the Report

- Bibliography
- Quoted Text
- Cited Text
- Small Matches (less than 8 words)

Match Groups

107 Not Cited or Quoted 11%
Matches with neither in-text citation nor quotation marks

0 Missing Quotations 0%
Matches that are still very similar to source material

0 Missing Citation 0%
Matches that have quotation marks, but no in-text citation

0 Cited and Quoted 0%
Matches with in-text citation present, but no quotation marks

Top Sources

9% Internet sources
8% Publications
0% Submitted works (Student Papers)

Integrity Flags

1 Integrity Flag for Review

Replaced Characters
63 suspect characters on 10 pages
Letters are swapped with similar characters from another alphabet.

Our system's algorithms look deeply at a document for any inconsistencies that would set it apart from a normal submission. If we notice something strange, we flag it for you to review.

A Flag is not necessarily an indicator of a problem. However, we'd recommend you focus your attention there for further review.

Match Groups

- 107 Not Cited or Quoted 11%
  Matches with neither in-text citation nor quotation marks
- 0 Missing Quotations 0%
  Matches that are still very similar to source material
- 0 Missing Citation 0%
  Matches that have quotation marks, but no in-text citation
- 0 Cited and Quoted 0%
  Matches with in-text citation present, but no quotation marks

Top Sources

- 9% Internet sources
- 8% Publications
- 0% Submitted works (Student Papers)

Top Sources

The sources with the highest number of matches within the submission. Overlapping sources will not be displayed.

1	Internet	mechanicalboost.com 1%
2	Internet	www.nepjol.info <1%
3	Internet	elibrary.tucl.edu.np <1%
4	Internet	ar.scribd.com <1%
5	Internet	www.linquip.com <1%
6	Internet	erepository.uonbi.ac.ke:8080 <1%
7	Internet	etd.aau.edu.et <1%
8	Internet	hdl.handle.net <1%
9	Internet	rguktrkvalley.files.wordpress.com <1%
10	Internet	worldwidescience.org <1%